

Official Journal of Turkish Society of Magnetic Resonance

# CRMRI

## Current Research in MRI

**Evaluation of the Presence of Additional Knee Pathology on Magnetic Resonance Imaging in Patients with Chondromalacia Patella**

Ömer Kaya, Okan Dilek, Duygu Özgül Özesen, Yunus Kenan Bıçakçı

**Effect of Serum Vitamin B12 Levels on Brain Volumes**

Hatice Cakir, Mukadder Sunar, Ozlem Celik Aydın, Osman Kagan CaKır

**pH-Sensitive, Encapsulated, and Natural Oral Contrast Media for Enterography**

Oktay Algin, Muharrem Olcer, Çağdas Oto

**Large Language Models on Magnetic Resonance Imaging Safety-Related Questions: Accuracy of ChatGPT-3.5, ChatGPT-4, Gemini, and Perplexity**

Esat Kaba, Hande Melike Bülbül, Gülen Burakgazi, Merve Solak, Serdar Tabakoğlu, Ayşenur Topçu Varlık, Nur Hürsoy, Fatma Beyazal Çeliker

## Editor in Chief

Mecit Kantarcı 

Department of Radiology, Erzincan Binali Yıldırım University, Faculty of Medicine; Atatürk University, Faculty of Medicine, Erzincan, Erzurum, Turkey

## Editors

### Abdominal Radiology

Aytekin Oto 

The University of Chicago, Department of Radiology, Chief Physician, Head of the Faculty Practice Plan and Dean for Clinical Affairs, Chicago, USA

Murat Danacı 

Department of Radiology, Ondokuz Mayıs University, Faculty of Medicine, Samsun, Turkey

### Breast Radiology

Serap Gültekin 

Department of Radiology, Gazi University, Faculty of Medicine, Ankara, Turkey

### Cardiac Radiology

Memduh Dursun 

Department of Radiology, İstanbul University, İstanbul Faculty of Medicine, İstanbul, Turkey

Cihan Duran 

Department of Diagnostic and Interventional Imaging, The University of Texas, McGovern Medical School, Texas, USA

### Emergency Radiology

Mehmet Ruhi Onur 

Department of Radiology, Hacettepe University Faculty of Medicine Hospital, Ankara, Turkey

### Engineer Group

Esin Öztürk Işık 

Biomedical Engineering, Boğaziçi University, İstanbul, Turkey

### Head & Neck Radiology

Nafi Aygün 

Department of Radiology, Johns Hopkins University School of Medicine, Baltimore, Maryland, USA

Hatice Gül Hatipoğlu 

Department of Radiology, Health Science University, Gulhane Faculty of Medicine, Ankara Bilkent City Hospital, Ankara, Turkey

### Musculoskeletal Radiology

Nil Tokgöz 

Department of Radiology, Gazi University, Faculty of Medicine, Ankara, Turkey

### Neuroradiology Radiology


Alpay Alkan 

Department of Radiology, Bezmialem Vakıf University, Faculty of Medicine, İstanbul, Turkey

### Pediatric Radiology

Korgün Koral 

Department of Radiology, University of Texas Southwestern Medical Center, Dallas, TX, USA

Süreyya Burcu Görkem 

Department of Pediatric Radiology, Adana State Hospital, Adana, Turkey

### Thorax Radiology

Polat Koşucu 

Department of Radiology, Karadeniz Teknik University, Faculty of Medicine, Trabzon, Turkey

### Biostatistical Consultant

Sonay Aydın 

Department of Radiology, Erzincan Binali Yıldırım University, Faculty of Medicine, Erzincan, Turkey



General Manager

Ali ŞAHİN

Finance Coordinator

Sinem Fehime KOZ

Journal Managers

Deniz KAYA

Irmak BERBEROĞLU

Publications Coordinators

Alara ERGİN

İrem ÖZMEN

Derya AZER

Nisanur ATICI

Şeref Mert GÜCÜN

Web Specialist

Erdem ERCİVAN

Sinem Fehime KOZ

Project Assistant

Batuhan KARA

Contact

Address: Büyükdere Cad. 199/6 34394

Mecidiyeköy, Şişli, İstanbul, Turkey

Phone: +90 212 217 17 00

E-mail: info@avesyayincilik.com

## About the Current Research in MRI

Current Research in MRI is a peer reviewed, open access, on-line-only journal published by the Turkish Society of Magnetic Resonance.

Current Research in MRI is a triannual journal that is published in English in April, August, and December.

### Indexing

Current Research in MRI is covered in the following indexing database;

- EBSCO

All content published in the journal is permanently archived in Portico.

### Aims, Scope, and Audience

Current Research in MRI aims to publish studies of the highest scientific and clinical value. It also encourages the submission of high-quality research in the field of radiology.

Current Research in MRI covers a wide range of topics related to radiology.

Current Research in MRI publishes original articles, reviews, case reports, and letters to the editor that are prepared in accordance with ethical guidelines.

The target audience of the journal includes healthcare professionals, physicians, and researchers who are interested in or working in the field of radiology.

You can reach the current version of the instructions to authors at <https://curremr.com/EN>

### Editor in Chief: Mecit Kantarcı

**Address:** Department of Radiology, Erzincan Binali Yıldırım University School of Medicine, Erzincan, Turkey

**E-mail:** akkanrad@hotmail.com

### Publisher: Turkish Society of Magnetic Resonance

**Address:** Konak Mah. 858. Sok. No: 2 Çakıroğlu İş Hanı Kat: 5 Daire: 55 Konak / İzmir, Turkey

### Publishing Services: AVES

**Address:** Büyükdere Cad., 199/6 34394 Şişli, İstanbul, Turkey

**Phone:** +90 212 217 17 00

**E-mail:** [info@avesyayincilik.com](mailto:info@avesyayincilik.com)

**Webpage:** [www.avesyayincilik.com](http://www.avesyayincilik.com)

## CONTENTS

### ORIGINAL ARTICLES

- 1 Evaluation of the Presence of Additional Knee Pathology on Magnetic Resonance Imaging in Patients with Chondromalacia Patella  
Ömer Kaya, Okan Dilek, Duygu Özgül Özesen, Yunus Kenan Bıçakçı
- 5 Effect of Serum Vitamin B12 Levels on Brain Volumes  
Hatice Cakir, Mukadder Sunar, Ozlem Celik Aydin, Osman Kagan Cakir
- 9 pH-Sensitive, Encapsulated, and Natural Oral Contrast Media for Enterography  
Oktay Algin, Muharrem Olcer, Çağdas Oto
- 16 Large Language Models on Magnetic Resonance Imaging Safety-Related Questions: Accuracy of ChatGPT-3.5, ChatGPT-4, Gemini, and Perplexity  
Esat Kaba, Hande Melike Bülbül, Gülen Burakgazi, Merve Solak, Serdar Tabakoğlu, Ayşenur Topçu Varlık, Nur Hürsoy, Fatma Beyazal Çeliker

### REVIEW

- 20 Advances in Machine Learning for Magnetic Resonance Imaging of Acute Ischemic Stroke: A Systematic Review  
Sena Azamat, Erdem Gürkaş, Esin Ozturk-Isik

### CASE REPORTS

- 27 Diagnosis of Caroli Disease with Gadoteric Acid-Enhanced Magnetic Resonance Imaging  
Ramazan Orkun Önder, Serdar Aslan, Tumay Bekci
- 30 A Rare Coupling: Central Tuberculous and Brucella Co-infection  
Önder Durmaz, Gönül Seven Yalçın, Umut Devrim Binay, Mecdi Gürhan Balci, Türkhun Çetin, Edhem Ünver

### LETTER TO THE EDITOR

- 33 Challenges in Magnetic Resonance Imaging Anesthesia Findings and Recommendations  
Hakan Gökalep Taş



# Evaluation of the Presence of Additional Knee Pathology on Magnetic Resonance Imaging in Patients with Chondromalacia Patella

Ömer Kaya<sup>1</sup> , Okan Dilek<sup>2</sup> , Duygu Özgül Özese<sup>3</sup> , Yunus Kenan Bıçakçı<sup>1</sup> 

<sup>1</sup>Department of Radiology, Cukurova University Faculty of Medicine, Adana, Turkey

<sup>2</sup>Department of Radiology, Health Sciences University Adana Faculty of Medicine, Adana, Turkey

<sup>3</sup>Department of Radiology, Cukurova State Hospital, Adana, Turkey

**Cite this article as:** Kaya Ö, Dilek O, Özgül Özese D, Bıçakçı YK. Evaluation of the presence of additional knee pathology on magnetic resonance imaging in patients with chondromalacia patella. *Current Research in MRI*, 2024;3(1):1-4.

**Corresponding author:** Ömer Kaya, e-mail: dr.omerkaya@gmail.com

**Received:** December 26, 2023 **Revision Requested:** January 30, 2024 **Last Revision Received:** January 30, 2024 **Accepted:** February 7, 2024

**Publication Date:** March 22, 2024

DOI:10.5152/CurrResMRI.2024.23087



Content of this journal is licensed under a Creative Commons Attribution-NonCommercial 4.0 International License.

## Abstract

**Objective:** Chondromalacia patella (CP) describes the softening of the patellar cartilage, and magnetic resonance imaging (MRI) is more useful in diagnosis than other imaging methods. The aim of study is to determine the frequency of other knee MRI findings and their relationship with chondromalacia stages in patients evaluated for reasons other than trauma and found to have patellar chondromalacia.

**Methods:** This retrospective study included patients who underwent knee MRI examination in the radiology departments of Cukurova University Faculty of Medicine and Health Sciences University Adana Faculty of Medicine for reasons other than trauma between January 2016 and January 2022. Magnetic resonance imaging was used to evaluate the presence and stage of CP, and the outerbridge system was used for staging. As additional findings, the presence of osteoarthritis, cruciate ligament, meniscus, collateral ligament, and patellar tendon pathologies were evaluated.

**Results:** A total of 278 patients, 168 women and 110 men, with an average age of  $59.4 \pm 9.8$  years, were included in our study. Forty-six patients had stage 1, 64 had stage 2, 66 had stage 3, and 102 had stage 4 CP. A statistically significant correlation was found between increasing chondromalacia stage and the presence and stage of osteoarthritis ( $P < .001$ ), the incidence of anterior cruciate ligament pathology ( $P < .001$ ), the incidence of tears of the medial meniscus (anterior horn  $P < .002$ , posterior horn  $P < .039$ ), and advanced age ( $P < .001$ ).

**Conclusion:** It has been determined that there is a relationship between the stage of CP and some additional knee pathologies and advanced age.

**Keywords:** Chondromalacia patella, knee MRI, additional findings

## INTRODUCTION

Chondromalacia patella (CP) is defined as the softening and degeneration of the hyalinized cartilage that forms the patellofemoral joint surface, which is the joint where the patellar bone meets the trochlear groove of the femur.<sup>1</sup> Chondromalacia patella presents with chronic anterior knee pain, which is one of the common complaints of admission to the hospital. It is one of the most common causes.<sup>2</sup> Although cartilage degeneration begins at an early age with cellular aging, it is known that some factors accelerate and facilitate the development of chondromalacia. Structural abnormalities in the patellofemoral and tibiofemoral joints may accelerate chondromalacia by increasing the load on the patellar cartilage. Other factors that facilitate the development of CP are trauma and inadequate vascular nutrition in the subchondral bone tissue.<sup>3,4</sup>

Although patellar cartilage evaluation is not fully possible with conventional radiography, it can be used to evaluate patellofemoral joint distance, joint osteoarthritis (OA) findings, and the presence of effusion. In lateral radiographs, changes in the subchondral bone can be noted.<sup>5-8</sup> It is known that plica and focal cartilage defects can be demonstrated with computed tomography arthrography, but its low sensitivity in showing early cartilage defects and the presence of ionizing radiation make magnetic resonance imaging (MRI) the preferred imaging modality for the diagnosis of CP.<sup>9-11</sup> The fact that it reveals the other soft tissue components of the knee joint, which is a complex structure along with the patellar cartilage, and their positional relationships with the joint in a multiplanar manner with high resolution has made MRI the most important examination in patients presenting with knee pain.<sup>12,13</sup> In recent years, fat-suppressed proton density/T2 sequence has come to the fore for the diagnosis of CP and has taken its place in routine knee MRI protocols.<sup>13</sup>

Chondromalacia patella is graded with a classification defined for arthroscopy by Outerbridge and then adapted radiologically via fat-suppressed proton density MR sequences.<sup>11</sup> In this classification, stage 0 is normal cartilage, stage 1 is focal hyperintensity in cartilage with normal contour, stage 2 is a focal defect affecting 50% or less of the cartilage thickness, stage 3 is chondromalacia affecting more than 50% of the cartilage thickness but not accompanied by bone marrow edema, stage 4 refers to a full-thickness cartilage defect that begins with edema in the subchondral bone and includes progressive bone changes.<sup>14</sup>

It is common to detect more than one pathology together in knee MRI examinations, and it is mentioned in the literature that other pathologies such as meniscopathy, ligament pathologies, and patellar tendinitis may accompany CP.<sup>15</sup> However, there is limited information about whether there is a relationship between the incidence of other knee pathologies and the stages of CP, and which knee pathologies and CP may frequently coexist. In this study, we investigated the existence and frequency of these associations.

## MATERIAL AND METHODS

The study is retrospective, and ethics committee approval was received from the Clinical Research Ethics Committee of Cukurova University Faculty of Medicine (number: 129, date: January 6). Since only MR images of the patients were used retrospectively in the study, informed consent was not obtained. Between January 2016 and January 2022, patients referred to the departments of radiology for knee MRI were screened. Patients with the presence of CP on fat-suppressed proton density axial MRI sequences were included in the study. Patients admitted due to trauma were excluded from the study. The cases included in the study were grouped into 4 stages according to the CP Outerbridge staging system (Figure 1). Additional pathologies, such as the presence and stage of OA, the presence of partial or full-thickness tear in the cruciate ligaments, the presence of degeneration or tear in the meniscus, the presence and stage of injury in the collateral ligaments, and the presence of patellar tendinitis, were recorded in the knee MRI examinations of 278 patients with CP.

The images included in the study were obtained on GE 3.0 Tesla SIGNA ARCHITECT and 1.5 Tesla OPTIMA MR (General Electric Healthcare, Milwaukee, Wisconsin, USA) devices and 3.0 and 1.5 Tesla INGENIA MR (PHILIPS, Eindhoven, Netherlands) devices. The non-contrast knee MRI protocol consisted of axial fat-suppressed proton density, sagittal, and coronal fat-suppressed T2 and sagittal T1-weighted sequences.

## Statistical Analysis

Chi-square or Fisher's exact test was performed for categorical variables. Kolmogorov-Smirnov test was applied to determine whether the numerical values were normally distributed. Kruskal-Wallis *H* test was applied to compare numerical values between groups.  $P < .05$  was considered statistically significant.

## RESULTS

A total of 278 patients, 168 women and 110 men, with an average age of  $59.4 \pm 9.8$  years, were included in our study. Forty-six of the patients had stage 1, 64 had stage 2, 66 had stage 3, and 102 had stage 4 patellar chondromalacia.

No significant statistical difference was detected in the frequency and distribution of chondromalacia stages between the right and left knees ( $P > .05$ ).

## MAIN POINTS

- Chondromalacia patella is a common cause of anterior knee pain.
- It may be associated with other knee pathologies.
- MRI is very successful in evaluation and it is useful to detect its association with other pathologies in order to ensure the rehabilitation of the patient.

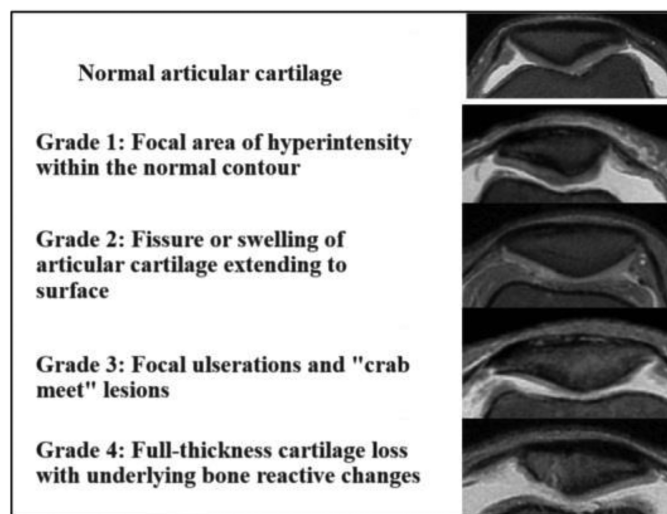


**Figure 1.** Outerbridge staging system on magnetic resonance images.

As the chondromalacia stage increases, the OA stage also progresses, and a linear and statistically significant relationship was detected between them ( $P < .05$ ).

A statistically significant relationship was found between the stage of chondromalacia and the rate of anterior cruciate ligament (ACL) involvement. This statistically significant difference arises from the difference between the rates of normal ACL presence in stage 1-2 chondromalacia cases and stage 4 chondromalacia cases (45% and 17%, respectively) and the difference between the rates of full-thickness tear in stage 1 chondromalacia cases and stage 3 chondromalacia cases (4% and 22%, respectively).

No statistically significant relationship was found between chondromalacia stage and posterior cruciate ligament (PCL) pathology ( $P > .05$ ).

A significant relationship was detected between medial meniscus (MM) anterior horn pathology and chondromalacia stage, and the presence of MM anterior horn pathology in stage 2 chondromalacia patients was found to be significantly lower than in other stages.

When looking at the relationship between MM posterior horn pathology and chondromalacia stage, there is a significant difference between the rates of patients with tears in stage 4 and 1 chondromalacia cases ( $P < .05$ ). As the chondromalacia stage progressed, an increase in the rate of tears in the MM posterior horn was detected.

No statistically significant relationship was found between the presence of lateral meniscus (LM) pathologies, collateral ligament (lateral collateral ligament and medial collateral ligament) pathologies, and patellar tendinitis and the stage of chondromalacia ( $P > .05$ ).

All findings are shown in Table 1.

## DISCUSSION

It is common for more than one support structure of the knee joint to be affected simultaneously. Accurate diagnosis and reporting of

**Table 1.** Statistical Relationship Between Chondromalacia and Additional Knee Magnetic Resonance Imaging Findings

	CHONDROMALACIA				P
	Stage 1 n=46	Stage 2 n=64	Stage 3 n=66	Stage 4 n=102	
<b>Knee</b>					
Right	19	27	38	52	.223 <sup>a</sup>
Left	27	37	28	50	
<b>Osteoarthritis</b>					
Stage 1	21	28	11	14	<.001 <sup>a</sup>
Stage 2	9	11	12	24	
Stage 3	10	8	17	24	
Stage 4	6	17	26	40	
<b>ACL</b>					
Normal	22	28	20	18	<.001 <sup>a</sup>
Partial tear	22	24	31	70	
Full thickness tear	2	12	15	14	
<b>PCL</b>					
Normal	41	59	56	86	.678 <sup>b</sup>
Partial tear	5	5	10	15	
Full thickness tear	-	-	-	1	
<b>MM-A</b>					
Normal	36	62	51	81	.002 <sup>b</sup>
Degeneration	2	1	4	1	
Tear	8	1	11	20	
<b>MM-P</b>					
Normal	18	19	18	15	.039
Degeneration	7	12	8	17	
Tear	21	33	40	70	
<b>LM-A</b>					
Normal	52	56	56	81	.625 <sup>b</sup>
Degeneration	1	1	1	4	
Tear	3	7	9	17	
<b>LM-P</b>					
Normal	42	63	61	91	.231 <sup>b</sup>
Degeneration	2	0	0	3	
Tear	2	1	5	7	
<b>MCL</b>					
Normal	40	52	43	71	.071 <sup>b</sup>
Stage 1	6	11	20	23	
Stage 2	0	1	3	7	
<b>LCL</b>					
Normal	45	64	66	96	.396 <sup>b</sup>
Stage 1	1	-	-	3	
Stage 2	-	-	-	2	
<b>Patellar Tendonitis</b>					
Absent	41	59	59	86	.300 <sup>a</sup>
Detected	3	5	7	16	
<b>Age (minimum–maximum)</b>	58.0 (39.0–76.0)	56.0 (38.0–77.0)	60.5 (40.0–82.0)	62.5 (47–79.0)	<.001 <sup>c</sup>

ACL, anterior cruciate ligament; LCL, lateral collateral ligament; LM-A, lateral meniscus anterior horn; LM-P, lateral meniscus posterior horn; MCL, medial collateral ligament; MM-A, medial meniscus anterior horn; MM-P, medial meniscus posterior horn; PCL, posterior cruciate ligament.

<sup>a</sup>Chi-square test.

<sup>b</sup>Fisher's exact test.

<sup>c</sup>Kruskal–Wallis *H* test.

accompanying pathologies affect patient management, treatment process, and prognosis.<sup>16</sup>

In a study conducted by Resorlu et al<sup>17</sup> evaluating the relationship between OA, CP, and MM tears, a positive correlation was found between OA, MM tears, and CP. According to the results of our study, it is noteworthy that as the CP stage increases, the frequency and stage of OA increases. Likewise, an increase in the frequency of tears in the anterior and posterior horns of MM was observed with increasing CP stages. Although chondromalacia is defined as the pathology on the patellar cartilage surface, it is thought that the resulting

deterioration in knee biomechanics increases the load on the menisci, especially MM, and facilitates the development of meniscopathy.<sup>18</sup>

No significant relationship was detected between LM pathologies and CP, which can be explained by the fact that MM pathologies are more common than LM, and MM is exposed to more load.<sup>19–21</sup>

The positive correlation between CP stage, which increased as the average age increased, was consistent with a similar study conducted by Ozel et al<sup>22</sup> It is thought that this situation may be related to cartilage degeneration that accelerates with cellular aging.

In another study investigating the co-occurrence of multiple knee joint pathologies, the positive correlation detected between CP and the presence of ACL injury and osteochondral lesion showed similar results to our study.<sup>23</sup>

No significant difference was found between PCL, collateral ligament pathologies, patellar tendinitis, and CP stages, and no study supporting the relationship between them and CP was found in the literature, consistent with our study.

As a conclusion, it is common for pathologies belonging to several supporting structures to be seen together in knee MRI examinations, and since their detection is important for the treatment process, the radiologist's awareness of accompanying pathologies is of critical importance in this process. According to the results of our study, the CP stage shows a positive correlation with advancing age, the presence of MM pathology, the frequency and stage of OA, and the presence of ACL pathology, and it is thought that it would be useful to evaluate the presence of these additional pathologies with MRI, especially in patients with advanced stage (stage 3 and 4) chondromalacia.

**Ethics Committee Approval:** Approval numbered 129, dated January 6, 2023, was received from the Ethics Committee of Çukurova University Faculty of Medicine.

**Informed Consent:** N/A.

**Peer-review:** Externally peer-reviewed.

**Author Contributions:** Concept – Ö.K., O.D., D.Ö.Ö.; Design – Ö.K., O.D., D.Ö.Ö.; Supervision – Ö.K., O.D., Y.K.B.; Resources – Ö.K., O.D.; Materials – Ö.K., O.D.; Data Collection and/or Processing – Ö.K., O.D.; Analysis and/or Interpretation – Ö.K.; Literature Search – Ö.K., D.Ö.Ö.; Writing Manuscript – Ö.K., D.Ö.Ö.; Critical Review – Ö.K., Y.K.B.

**Declaration of Interests:** The authors have no conflict of interest to declare.

**Funding:** The authors declared that this study has received no financial support.

## REFERENCES

- Gagliardi JA, Chung EM, Chandnani VP, et al. Detection and staging of chondromalacia patellae: relative efficacies of conventional MR imaging, MR arthrography, and CT arthrography. *AJR Am J Roentgenol.* 1994; 163(3):629-636. [\[CrossRef\]](#)
- Schiavone-Panni A, Perisano C, Del-Regno C, Corona K. Anterior knee pain. *Arthrosc Sport Inj Appl High-Level Athletes.* 2016;373-379.
- Duran S, Cavusoglu M, Kocadal O, Sakman B. Association between trochlear morphology and chondromalacia patella: an MRI study. *Clin Imaging.* 2017;41:7-10. [\[CrossRef\]](#)
- Tuna BK, Semiz-Oysu A, Pekar B, Bukte Y, Hayirlioglu A. The association of patellofemoral joint morphology with chondromalacia patella: a quantitative MRI analysis. *Clin Imaging.* 2014;38(4):495-498. [\[CrossRef\]](#)
- Grelsamer RP, Bazos AN, Proctor CS. Radiographic analysis of patellar tilt. *J Bone Joint Surg Br.* 1993;75(5):822-824. [\[CrossRef\]](#)
- Dowd GS, Bentley G. Radiographic assessment in patellar instability and chondromalacia patellae. *J Bone Joint Surg Br.* 1986;68(2):297-300. [\[CrossRef\]](#)
- Aglietti P, Insall JN, Cerulli G. Patellar pain and incongruence: I: Measurements of incongruence. *Clin Orthop Relat Res.* 1983;(176):217-224.
- Carson WG Jr, James SL, Larson RL, Singer KM, Winternitz WW. Patellofemoral disorders: physical and radiographic evaluation: Part I: Physical examination. *Clin Orthop Relat Res.* 1984;(185):165-177.
- Baysal O, Baysal T, Alkan A, Altay Z, Yologlu S. Comparison of MRI graded cartilage and MRI based volume measurement in knee osteoarthritis. *Swiss Med Wkly.* 2004;134(19-20):283-288. [\[CrossRef\]](#)
- Pihlajamäki HK, Kuikka PI, Leppänen VV, Kiuru MJ, Mattila VM. Reliability of clinical findings and magnetic resonance imaging for the diagnosis of chondromalacia patellae. *J Bone Joint Surg Am.* 2010;92(4):927-934. [\[CrossRef\]](#)
- Crema MD, Roemer FW, Marra MD, et al. Articular cartilage in the knee: current MR imaging techniques and applications in clinical practice and research. *RadioGraphics.* 2011;31(1):37-61. [\[CrossRef\]](#)
- Yang B, Tan H, Yang L, Dai G, Guo B. Correlating anatomy and congruence of the patellofemoral joint with cartilage lesions. *Orthopedics.* 2009;32(1):20. [\[CrossRef\]](#)
- Ali SA, Helmer R, Terk MR. Analysis of the patellofemoral region on MRI: association of abnormal trochlear morphology with severe cartilage defects. *AJR Am J Roentgenol.* 2010;194(3):721-727. [\[CrossRef\]](#)
- Brittberg M, Winalski CS. Evaluation of cartilage injuries and repair. *J Bone Joint Surg Am.* 2003;85-A(suppl 2):58-69. [\[CrossRef\]](#)
- Lu W, Yang J, Chen S, Zhu Y, Zhu C. Abnormal patella height based on Insall-Salvati ratio and its correlation with patellar cartilage lesions: an extremity-dedicated low-field magnetic resonance imaging analysis of 1703 Chinese cases. *Scand J Surg.* 2016;105(3):197-203. [\[CrossRef\]](#)
- Vincken PW, ter Braak BP, van Erkel AR, et al. Effectiveness of MR imaging in selection of patients for arthroscopy of the knee. *Radiology.* 2002;223(3):739-746. [\[CrossRef\]](#)
- Resorlu M, Doner D, Karatag O, Toprak CA. The relationship between chondromalacia patella, medial meniscal tear and medial periarticular bursitis in patients with osteoarthritis. *Radiol Oncol.* 2017;51(4):401-406. [\[CrossRef\]](#)
- Aktas B, Komut E, Kultur T. The relationship between patellar tendon height (Patella alta and Patella baja) and patellar chondromalacia. *KUTF Journal.* 2015;17:1-8.
- Rath E, Richmond JC. The menisci: basic science and advances in treatment. *Br J Sports Med.* 2000;34(4):252-257. [\[CrossRef\]](#)
- Metcalfe MH, Barrett GR. Prospective evaluation of 1485 meniscal tear patterns in patients with stable knees. *Am J Sports Med.* 2004;32(3):675-680. [\[CrossRef\]](#)
- Englund M, Guermazi A, Gale D, et al. Incidental meniscal findings on knee MRI in middle-aged and elderly persons. *N Engl J Med.* 2008; 359(11):1108-1115. [\[CrossRef\]](#)
- Özel D, Kır MÇ, Öncü M. Evaluation of correlation between clinical and magnetic resonance findings of patellar chondromalacia. *Haydarpaşa Numune J.* 2020;60:221-225.
- Avcu S, Altun E, Akpınar I, Bulut MD, Eresov K, Biren T. Knee joint examinations by magnetic resonance imaging: the correlation of pathology, age, and sex. *N Am J Med Sci.* 2010;2(4):202-204. [\[CrossRef\]](#)



# Effect of Serum Vitamin B12 Levels on Brain Volumes

Hatice Cakir<sup>1</sup>, Mukadder Sunar<sup>1</sup>, Ozlem Celik Aydin<sup>2</sup>, Osman Kagan Cakir<sup>3</sup>

<sup>1</sup>Department of Anatomy, Erzincan Binali Yildirim University Faculty of Medicine, Erzincan, Turkey

<sup>2</sup>Department of Pharmacology, Erzincan Binali Yildirim University Faculty of Medicine, Erzincan, Turkey

<sup>3</sup>Department of Family Medicine, Erzincan Binali Yildirim University Faculty of Medicine, Erzincan, Turkey

**Cite this article as:** Cakir H, Sunar M, Celik Aydin O, Cakir O.K Effect of serum vitamin B12 levels on brain volumes. *Current Research in MRI*, 2024;3(1):5-8.

**Corresponding author:** Osman Kagan Cakir, e-mail: dr.kagancakir@gmail.com

**Received:** January 30, 2024 **Revision Requested:** February 12, 2024 **Last Revision Received:** February 13, 2024 **Accepted:** February 19, 2024

**Publication Date:** March 28, 2024

DOI:10.5152/CurrResMRI.2024.24092



Content of this journal is licensed under a Creative Commons Attribution-NonCommercial 4.0 International License.

## Abstract

**Objective:** To research the relationship between brain volumes and serum vitamin B12 markers.

**Methods:** To investigate the volume changes of serum vitamin B12 markers in brain magnetic resonance imaging measurements of 62 participants admitted to the clinic.

**Results:** Volumes were significantly higher in vitamin B12 users compared to non-users. Vitamin B12 and white matter volumes increase together with a strong relationship and significantly.

**Conclusion:** Levels of vitamin B12 can influence the brain using multiple mechanisms. Low vitamin B12 status increases the likelihood of brain atrophy and may even be a factor in cognitive decline.

**Keywords:** Vitamin B12, brain volumes, magnetic resonance imaging, white matter volumes, gray matter volumes, lobes volumes

## INTRODUCTION

Vitamin B12 is an essential water-soluble vitamin and is involved in hematopoiesis, nervous system function, maintenance of gastrointestinal continuity and regulation of metabolic processes. A deficiency in vitamin B12 is linked to epithelial alterations in the gastrointestinal mucosa, neurological and psychiatric disorders, and hematopoietic disorders affecting erythrocyte formation.<sup>1</sup> The primary indicator in the diagnosis of vitamin B12 deficiency is changes in the hematopoietic system.<sup>2</sup> Furthermore, neurological disorders are often the earliest and in some cases the only clinical manifestations of a functional vitamin B12 deficiency.<sup>3</sup> Between 75% and 90% of people with clinically significant B12 deficiency have neurologic disorders, and in approximately 25% of cases these are the only clinical manifestations of B12 deficiency.<sup>4-6</sup> Vitamin B12's neurological importance is intimately associated with its regulatory mechanisms about brain development and function. Vitamin B12 deficiency can cause several neurological symptoms, including paresthesia, numbness on the skin, impaired coordination, and slowed nerve conduction velocity. Deficits in vitamin B12, particularly in older adults, can negatively affect on brain volume. Progressive brain atrophy in the elderly has been linked to vitamin B12 deficiency.<sup>7</sup> The relationship between brain volume and vitamin B12 has been studied, and significant findings have been made. Low levels of vitamin B12 were found to be significantly correlated with the rate at which brain volume was decreasing. A lower brain volume has been linked to lower levels of vitamin B12 and holotranscobalamin and higher levels of total homocysteine and methylmalonic acid.<sup>8</sup> Vitamin B12 and total homocysteine levels are said to be associated with accelerated brain aging in older adults. It highlights the need for randomized clinical trials to determine whether vitamin B12 supplementation is essential in slowing brain aging.<sup>9</sup> The possible correlation between brain volume and vitamin B12 may be crucial for preserving cognitive function in elderly individuals. However, it should be noted that there are different findings in the existing literature. In a different investigation, DTI revealed microstructural alterations in the white matter regions of patients who were vitamin B12 deficient, although conventional MR imaging revealed no abnormalities.<sup>10</sup> Our study's objective was to thoroughly investigate the connection between vitamin B12 levels and brain volume. The correlation between brain capacity and vitamin B12 levels is complicated and multidimensional. Low B12 levels may negatively affect brain volume, according to current studies; however, the precise mechanism and clinical implications of this effect are yet unclear.

Our study aims to fill the existing knowledge gap in this field by examining the relationship between vitamin B12 levels and brain volume in more detail. Our research holds particular significance in identifying the function of vitamin B12 in safeguarding brain health within the community. Our study's findings could have a significant impact on clinical procedures for the early detection and treatment of vitamin B12 deficiency and could help create new strategies to stop brain atrophy in the general population.

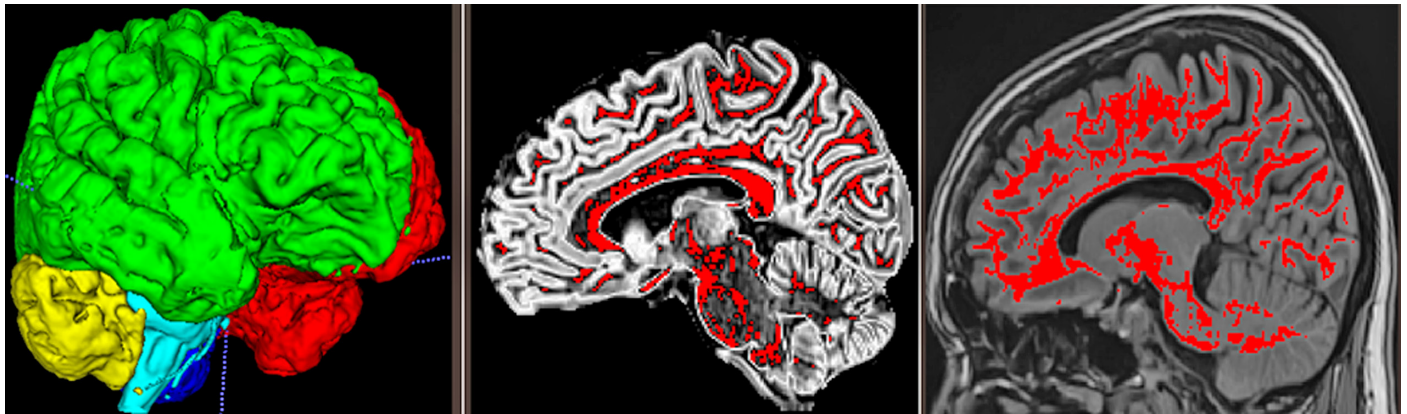


**Figure 1.** Fully-automated lobes, gray matter, white matter segmentation by volBrain.

## MATERIAL AND METHODS

### Participants

In our study, we retrospectively reviewed the images and serum vitamin B12 levels of 62 adult patients. All participants were informed in writing and informed consent was obtained. Approval for the study was obtained from Erzincan Binali Yıldırım University Clinical Research Ethics Committee (Ethics Committee decision date: November 30, 2023; Decision number: 2023-21/1) The study was conducted on human participants at Menguçk Gazi Training and Research Hospital. All procedures performed in this study complied with the ethical standards of the institution. The MRI used in the study is ethically and scientifically safe.

The study group consisted of healthy 24 volunteers who had used vitamin B12 within the last 1 year and healthy 38 volunteers who had not used vitamin B12 within the last 1 year, and were selected without a history of brain surgery or trauma, neurologic or psychiatric disease or substance abuse. Our study group consisted of 62 participants. There were 7 men and 55 women among the participants. The average age was 37.21 years (min-max 19-59 years).

### Magnetic Resonance Imaging Protocol and Segmentation Method

The MRI used in the study was performed with a high-resolution magnetic resonance device (1.5 T Siemens Aera scanner, Germany). The measurements were performed as TR (repetition time) /TE (echo Time), 2200/2.67ms; flip angle 8; acquisition matrix, 256 × 246; FOV, 250X250 mm; acquisition time, 4 minutes 59 seconds; number of axial slices, 192; slice thickness=1 mm (with no gap) in T1 weighted 3D Magnetization Prepared Rapid Gradient Echo sequence covering the whole brain.

Magnetic resonance imaging data processing and total brain, white matter, gray matter, thalamus, hippocampus, frontal lobe, temporal lobe, parietal lobe, occipital lobe, volumetric analyses were performed

using volBrain (v.1.0, <http://volbrain.upv.es>), a free online MRI brain volumetry system. volBrain is a fully automated segmentation technique of which the algorithm is based on multi-atlas patch-based label fusion segmentation technology (Figure 1).<sup>11</sup>

### Statistical Analysis

IBM SPSS™ Version 22 (IBM SPSS Corp.; Armonk, NY, USA) program was used for statistical evaluation of the analyses. The normality of data distribution was assessed using the Kolmogorov–Smirnov test. One-way analysis of variance test and independent *t*-test were used to compare the age, gender, and brain volume variables between the group using vitamin B12 in the last year and the group not using vitamin B12 in the last year. Descriptive statistical methods (frequency, percentage, mean, standard deviation) were used to evaluate the study data. Partial correlation analysis was used to correlate volumetric measurements with vitamin B12 levels and brain volumes. A value of  $p \leq .05$  was considered statistically significant for the results.

## RESULTS

The median age of participants was 37.21 years (min-max 19-59 years) respectively. White matter, gray matter, total brain, thalamus, hippocampus, frontal lobe, temporal lobe, parietal lobe, occipital lobe volumes were significantly higher in vitamin B12 users compared to nonusers ( $p < .05$  for all, Table 1). Correlation analysis was performed to determine the relationship between vitamin B12 and total brain volume, white matter volume, gray matter volume, thalamus volume,

**Table 1.** Comparison of Volumes of Different Brain Regions According to Groups

	Not Using B12 Group (n=38)		Using B12 Group (n=24)		<i>p</i>
	Mean (cm <sup>3</sup> )	SD (cm <sup>3</sup> )	Mean (cm <sup>3</sup> )	SD (cm <sup>3</sup> )	
White matter	420.10	27.74	497.20	45.56	<.001**
Gray water	613.91	41.97	681.46	51.02	<.001**
Total brain	1034.01	59.54	1178.66	87.97	<.001**
Thalamus	10.51	0.78	11.85	0.90	<.001**
Hippocampus	7.44	0.60	8.00	0.61	.001*
Frontal lobe	151.80	14.95	169.24	16.18	<.001**
Temporal lobe	102.55	9.41	115.20	8.48	<.001**
Parietal lobe	91.94	7.49	104.04	9.81	<.001**
Occipital lobe	67.59	6.29	74.30	7.32	.001*

SD, standard deviation.

\**P*-value < .05 significant.

\*\**P*-value < .001 highly significant.

### MAIN POINTS

- Vitamin B12's neurological importance is intimately associated with its regulatory mechanisms about brain development and function.
- Low vitamin B12 status increases the likelihood of brain atrophy and may even be a factor in cognitive decline.
- Vitamin B12 and white matter volumes increase together with a strong relationship and significance.
- Brain volumes were significantly higher in vitamin B12 users compared to nonusers.

**Table 2.** Association of Different Brain Regions with Vitamin B12

		Correlations						Frontal lobe	Temporal Lobe	Parietal Lobe	Occipital Lobe
	B12	White Matter	Graywater	Brain	Thalamus	Hippocampus					
B12	<i>r</i>	1									
	<i>p</i>										
White matter	<i>r</i>	.287*	1								
	<i>p</i>	.024									
Graywater	<i>r</i>	.177	.736	1							
	<i>p</i>	.169	.000								
Brain	<i>r</i>	.247	.926	.937	1						
	<i>p</i>	.053	.000	.000							
Thalamus	<i>r</i>	.207	.716	.839	.837	1					
	<i>p</i>	.107	.000	.000	.000						
Hippocampus	<i>r</i>	.125	.530	.664	.643	.493	1				
	<i>p</i>	.333	.000	.000	.000	.000					
Frontal lobe	<i>r</i>	.174	.640	.901	.833	.782	.599	1			
	<i>p</i>	.177	.000	.000	.000	.000	.000				
Temporal lobe	<i>r</i>	.150	.707	.845	.836	.683	.478	.705	1		
	<i>p</i>	.243	.000	.000	.000	.000	.000	.000			
Parietal lobe	<i>r</i>	.181	.752	.935	.909	.815	.645	.826	.788	1	
	<i>p</i>	.158	.000	.000	.000	.000	.000	.000	.000		
Occipital lobe	<i>r</i>	.113	.614	.805	.765	.608	.582	.664	.615	.791	1
	<i>p</i>	.383	.000	.000	.000	.000	.000	.000	.000	.000	

\*Correlation is significant at the 0.05 level (2-tailed).

hippocampus volume, frontal lobe volume, temporal lobe volume, parietal lobe volume, occipital lobe volume. As a result of the statistics; a strong positive and significant relationship was found between vitamin B12 and white matter volumes. In other words, vitamin B12 and white matter volumes increase together with a strong relationship and significantly ( $p < .05$ , Table 2).

## DISCUSSION

Our study showed that brain volumes were larger in the group that had used vitamin B12 in the last 1 year compared to the group that had not used vitamin B12 in the last 1 year. Brain volumetric measurements were positively correlated with serum vitamin B12 supplementation. However, there was also a correlation found between increased brain volume and higher vitamin B12 levels. Our study suggests a beneficial effect of vitamin B12 supplementation for brain volumes; in contrast to the group that did not get vitamin B12 supplements, the group that took vitamin B12 supplements in our research had larger brain volumes. An investigation revealed correlations between different markers of vitamin B12, white matter lesions, and cognitive performance.<sup>12</sup> In our study, a strong positive and significant correlation was found between vitamin B12 and white matter volumes. Patients with vitamin B12 deficiency or disease affecting vitamin B12 metabolism have been shown to demonstrate areas of demyelination on brain MRI.<sup>13,14</sup> Consequently, our results provide credence to the idea that low vitamin B12 status increases the likelihood of brain atrophy and may even be a factor in cognitive decline.

This study elucidates the relationship between vitamin B12 supplementation and brain volume, indicating a positive influence, particularly on white matter volume. However, the connection between B12 deficiency and brain health is multifaceted and intricate. While our results suggest a potential link between brain volume variations and B12 levels, they underscore the need for more in-depth exploration of the underlying mechanisms.

In conclusion, our study suggests a beneficial effect of vitamin B12 supplementation on brain volume. However, comprehensive studies involving larger, demographically diverse cohorts are essential for a clearer understanding of the relationship between vitamin B12 supplementation and brain health, potentially solidifying the benefits of B12 supplementation for brain health in the broader population.

## Study Limitations

The study is constrained by a limited participant number, an imbalance in gender distribution, and its execution in a single hospital, which may limit the applicability of findings to the general population. These limitations should be taken into consideration when interpreting the results. Future research, conducted with larger and more diverse populations across various locations, would enhance the generalizability of our findings.

**Ethics Committee Approval:** Erzincan Binali Yıldırım University Clinical Research Ethics Committee (Ethics Committee decision date: November 30, 2023; decision number: 2023-21/1).

**Informed Consent:** Written informed consent was obtained from patients who participated in this study.

**Peer-review:** Externally peer-reviewed.

**Author Contributions:** Concept – H.C.; Design – H.C.; Supervision – H.C., O.K.C.; Resources – H.C., M.S.; Materials – H.C.; Data collection and/or Processing – O.C.A., O.K.C.; Analysis and/or Interpretation – O.K.C., M.S., O.C.A.; Literature Search – H.C., M.S.; Writing Manuscript – M.S., O.K.C.; Critical Review – O.C.A., O.K.C.; Other – M.S.

**Declaration of Interests:** The authors have no conflict of interest to declare.

**Funding:** The authors declared that this study has received no financial support.

## REFERENCES

- Gröber U. Interactions between drugs and micronutrients. *Med Monatsschr Pharm.* 2006;29(1):26-35. [\[CrossRef\]](#)

2. Stabler SP. Clinical practice. Vitamin B12 deficiency. *N Engl J Med*. 2013;368(2):149-160. [\[CrossRef\]](#)
3. Green R. Vitamin B12 deficiency from the perspective of a practicing hematologist. *Blood*. 2017;129(19):2603-2611. [\[CrossRef\]](#)
4. Gröber U. Micronutrients: metabolic tuning-prevention-therapy. *Drug Metab Drug Interact*. 2009;24(2-4):331-. [\[CrossRef\]](#)
5. Allen LH. How common is vitamin B-12 deficiency? *Am J Clin Nutr*. 2009;89(2):693S-696S. [\[CrossRef\]](#)
6. Food IoM, Intakes NBSCotSEoDR. *Dietary Reference Intakes for Thiamin, Riboflavin, Niacin, Vitamin B6, Folate, Vitamin B12, Pantothenic Acid, Biotin, and Choline*. Washington, DC: National Academy Press; 2000.
7. Gröber U, Kisters K, Schmidt J. Neuroenhancement with vitamin B12—underestimated neurological significance. *Nutrients*. 2013;5(12):5031-5045.
8. Vogiatzoglou A, Refsum H, Johnston C, et al. Vitamin B12 status and rate of brain volume loss in community-dwelling elderly. *Neurology*. 2008;71(11):826-832. [\[CrossRef\]](#)
9. Hooshmand B, Mangialasche F, Kalpouzos G, et al. Association of vitamin B12, folate, and sulfur amino acids with brain magnetic resonance imaging measures in older adults: a longitudinal population-based study. *JAMA Psychiatry*. 2016;73(6):606-613. [\[CrossRef\]](#)
10. Gupta S, Girshick R, Arbeláez P, Malik J, eds. *Learning rich features from RGB-D images for object detection and segmentation*. *Computer Vision—ECCV 2014*. Proceedings, Part VII: 13th European Conference, Zurich, Switzerland, Springer, Berlin; 2014.
11. Manjón JV, Coupé P. volBrain: an online MRI brain volumetry system. *Front Neuroinform*. 2016;10:30. [\[CrossRef\]](#)
12. de Lau LM, Smith AD, Refsum H, Johnston C, Breteler MM. Plasma vitamin B12 status and cerebral white matter lesions. *J Neurol Neurosurg Psychiatry*. 2009;80(2):149-157. [\[CrossRef\]](#)
13. Smith AD, Smith SM, De Jager CA, et al. Homocysteine-lowering by B vitamins slows the rate of accelerated brain atrophy in mild cognitive impairment: a randomized controlled trial. *PLoS One*. 2010;5(9):e12244. [\[CrossRef\]](#)
14. Scalabrino G. Cobalamin (vitamin B12) in subacute combined degeneration and beyond: traditional interpretations and novel theories. *Exp Neurol*. 2005;192(2):463-479. [\[CrossRef\]](#)



# pH-Sensitive, Encapsulated, and Natural Oral Contrast Media for Enterography

Oktaý Algin<sup>1,3</sup> , Muharrem Olcer<sup>4</sup> , Çagdas Oto<sup>5,6</sup> 

<sup>1</sup>Interventional MR Clinical R&D Institute, Ankara University, Ankara, Turkey

<sup>2</sup>Department of Radiology, Ankara University Faculty of Medicine, Ankara, Turkey

<sup>3</sup>National MR Research Center, Bilkent University, Ankara, Turkey

<sup>4</sup>Department of Pharmaceutical Technology, Afyonkarahisar University Faculty of Pharmacy, Afyonkarahisar, Turkey

<sup>5</sup>Department of Anatomy, Ankara University Veterinary Faculty, Ankara, Turkey

<sup>6</sup>Medical Design Research and Application Center, Ankara University, Ankara, Turkey

**Cite this article as:** Algin O, Olcer M, Oto Ç. PH-sensitive, encapsulated, and natural oral contrast media for enterography. *Current Research in MRI*, 2024;3(1):9-15.

**Corresponding author:** Oktaý Algin, e-mail: droktayalgin@gmail.com

**Received:** February 7, 2024 **Accepted:** March 5, 2024 **Publication Date:** April 22, 2024

DOI:10.5152/CurrResMRI.2024.24073



Content of this journal is licensed under a Creative Commons Attribution-NonCommercial 4.0 International License.

## Abstract

**Objective:** The aim was to provide a more efficient and tolerable oral contrast agent for bowel distension with fewer side effects due to its pH-sensitive nature.

**Methods:** Mixtures of uncoated powder and enteric-coated granule forms of locust bean and xanthan gum (LBXG, 1 : 1 ratio) were developed. Locust bean and xanthan gum and commercially available oral contrast agents were examined using 3-tesla MR and MDCT units to determine imaging characteristics. In addition, LBXG was tested in a rabbit by a 3-tesla MR system.

**Results:** Enteric-coated LBXG had a minimum of 10 times water absorption and swelling in the intestinal environment (pH 4.5-7.4). The lactulose solution was hyperdense, and the other contrast agents (including LBXG) were isodense on CT images. Methylcellulose solutions showed clumping in all environments despite sufficient shaking, and this type of clumping was not observed in other solutions. All solutions were hypointense on T1-weighted images and hyperintense on T2-weighted MR images. Although the enteric-coated LBXG granules were homogeneously soluble in water and an alkaline environment, they did not dissolve and precipitated in the acidic buffer despite sufficient shaking. LBXG showed biphasic character on MR images of the rabbit.

**Conclusion:** Enteric-coated LBXG granules may be an effective oral contrast agent for enterography examinations. Because of its target-specific nature, it may provide fewer side effects and a higher diagnostic efficiency/tolerance capacity. It can be used for enterography exams and bowel cleansing before enterography, endoscopy, and/or surgery.

**Keywords:** Enterography, distension, bowel cleaner, oral contrast agent, CT, MRI

## INTRODUCTION

Adequate small bowel distension is essential for optimal acquisition of CT or MR enterography examinations.<sup>1</sup> Collapsed bowel segments may hide abnormalities or mimic pathological conditions on enterography images.<sup>2</sup> Several oral contrast agents have been used to provide adequate small bowel distension.<sup>3</sup> The most commonly used compounds are biphasic ones (such as polyethylene glycol, lactulose, methylcellulose, sorbitol, and/or mannitol).<sup>4</sup> However, all these oral contrast agents have disadvantages.<sup>5</sup> For example, methylcellulose has a high risk of clumping during preparation or drinking difficulties due to unpleasant smells. Others have dose-dependent side effects such as abdominal pain, cramping, vomiting, and excessive diarrhea. In addition, the tolerability and efficacy of these agents are limited. In summary, the question of which oral contrast agent is optimal for enterography remains unresolved. Therefore, novel oral contrast agents must be developed to overcome these limitations.

We developed a new pH-sensitive, natural, and nonabsorbable oral contrast medium containing locust bean and xanthan gum (LBXG) for enterography examinations. The recipe for the tested beverage has been deposited as a patent. We investigated the features of this oral contrast agent in various in vitro and in vivo experiments.

## MATERIAL AND METHODS

Eudragit® L 100 and 12.5 (methacrylic acid, methyl methacrylate; 1 : 1; Evonik Industries, Essen, Germany) were used as the enteric polymer. Ethanol 95% (Vins Industries OOD, Bulgaria), sodium hydroxide (Emplura Merck, Germany), hydrochloric acid (Emsure ACS, ISO, Reag. Ph Eur. Sigma-Aldrich, Austria), disodium hydrogen phosphate (Emsure ACS, Reag. Ph Eur. Merck, Germany), acetone (Emir Chemistry, Turkey), and sodium hydrogen phosphate (Emsure ACS, Reag. Ph Eur. Merck, Germany) were used as analytical grade and as received without any further purification. The rabbit experiment was approved by the Partners Healthcare Institutional Animal Care and Use Committee and was conducted

under its guidelines. Our ethical board approval date and number for this study from the Ethics Committee of Veterinary Faculty, Ankara University (22nd August 2022, Number: 2022/16).

### Procedures for the Preparation of Enteric-Coated Granules

Enteric-coated LBXG granules were prepared using the wet granulation method. Eudragit® L100 was dissolved in a mixture of ethanol and acetone (1 : 1). As a result, a 30% Eudragit® L100 solution was obtained. The required quantities of LBXG (Shausan Chemicals and Drugs, Mumbai, India) were weighed, mixed, and sifted through an ASTM No. 20 mesh (850 µm) sieve. Subsequently, the blend was mixed using a dry rotary mixer. Enteric-coated LBXG granules were then prepared in a rapid mix granulator. LBXG was accurately weighed, mixed, and sifted through an ASTM No. 40 mesh (425 µm) sieve. Granules were prepared using the wet granulation technique. Ethyl alcohol and acetone were used as the granulation fluid. The LBXG components were mixed with 30% Eudragit® L100 in a mixture of ethanol and acetone (1 : 1). The wet mass was passed through an ASTM No. 12 mesh (1.7 mm) sieve, and the resulting granules were dried at 50°C in an oven dryer until a loss of 0.5%-1% on drying (LOD). The amount of enteric polymer was approximately 10% based on the total weight of the powder mixture. Dried granules were further passed through an oscillating granulator using an ASTM No. 18 mesh (1 mm) sieve. The sieved and dried granules were then packed into moisture-proof polypropylene–polyethylene (PP/PE) bags.

### Characterization and Analysis of Enteric-Coated Granules

The following tests were performed on the coated granules:

**General appearance:** the granule size, shape, color, and texture of the granule surface are visually defined.

**Weight change:** the loading capacity of the enteric coating agent is calculated by considering the weight of the powder mass. Before and after the granulation procedures, the weight of the granules was measured. The amount of enteric coating agent loaded into the LBXG powder was defined. The target ratio was chosen as 10% ± 0.5.

**Water content:** Approximately 38 mL methanol was transferred to the titration vessel and titrated with Karl Fischer reagent to the electrometric endpoint. A total of 300 mg of the powder was accurately weighed and transferred into the titration vessel, mixed, and titrated with the Karl Fischer titration reagent to the electrometric endpoint. The water content of the powder was calculated using the following formula:

Calculate the percentage of water in the sample as follows:

Percentage of water in weighed samples =  $(V_r \times F \times 100) / W_s$

$F$  = water equivalence of the Karl Fischer reagent

$V_r$  = mL of Karl Fischer reagent used, and  $W_s$  = weight of the sample in mg.

**Acid resistance test:** enteric-coated LBXG granules were kept for 1 hour at 37°C ± 0.5 using a 20-rpm shaker at a pH 1.2 medium. In addition, the viscosity of the solution was measured. The same experiments and conditions were repeated in a pH 7.4 medium, in the following step. Finally, the viscosities of the solutions were measured using a digital viscometer (Brookfield DV-I prime, USA).

**Particle size and distribution:** enteric-coated LBXG granules were dispersed in glycerin. The particle sizes and distributions were examined under a microscope.

**Viscosity values in various media:** the locust bean and xanthan gum were mixed in a one-to-one ratio for all experiments. The uncoated powder and the coated granule forms of the LBXG were dissolved in water, pH 1.2, pH 7.4, and their viscosities were measured. Diluted suspensions of 0.5%, 1%, 2%, 2.5%, and 3% were obtained using distilled water, 0.1 N hydrochloric acid, and phosphate (pH 7.4) buffer. The viscosity values of these diluted mixtures were calculated depending on the mixing time/speed, resistance, viscosity, and concentration.

### Imaging Exams

Commercially available oral contrast agents [(polyethylene-glycol (PEG), lactulose (Duphalac), carboxy-methylcellulose (CMC)] in our country and LBXG mixtures with different buffers (distilled water, acidic, and alkaline pH) and various concentrations (0.5%, 1.0%, 2.0%, 2.5%, and 3.0%) were placed in annotated plastic tubes. The concentrations of these solutions were the same as those per mL in routine enterography examinations. The tubes were evaluated using a 3-tesla (3T) MR unit (Trio, Siemens, Erlangen, Germany) and a 32-channel birdcage head coil. Multi-detector computed tomography (128-detector, Revolution Evo, GE, USA) images with 1 mm<sup>3</sup> voxel sizes were also obtained.

In addition, LBXG was tested in vivo in a rabbit experiment. One hundred milliliters of a 1% LBXG solution prepared using cherry juice was administered using a 6-French nasogastric catheter. The injection rate of the LBXG solution was 20 mL/min. After 100 mL of LBXG injection, the rabbit's abdominopelvic region was scanned with a 15-channel transmit/receive type birdcage knee coil and the same 3T MR device. Acquisition details of the 3T MR exams are given in Table 1.

## RESULTS

### Appearance

The powder form of the LBXG mixture turned into a granular structure after coating with Eudragit®. The average particle size increased approximately 100 times. The powder and granular forms of LBXG are shown in Figure 1.

### Weight Change

The loading capacity of the enteric coating material, the weight of the powder mass (before granulation), and the weight of the granules (obtained after granulation) were calculated by considering the amount of enteric coating material loaded into the system. In terms of production efficiency, a loss of up to 5% in the total powder mass was observed. However, in the amount of Eudragit covered in the powder, the target was 10% ± 0.5; while 9.5%-10.5%, the amount of Eudragit

### MAIN POINTS

- The enteric-coated LBXG granules might be an effective oral contrast agent for the enterography exams.
- The enteric-coated LBXG granules may provide fewer side effects and a higher diagnostic efficiency/tolerance capacity.
- The enteric-coated LBXG granules can be used for image acquisition of enterography exams and optimal bowel cleansing before the enterography, endoscopy, and/or surgery.

**Table 1.** 3-Tesla MRE Protocol of the Experiments

Sequences/Parameters	3D-T2W (TSE)	2D-T1W (GRE)	3D-T1W (GRE)	2D-T1W (TSE)	2D-T2W (TSE)
TR/TE (ms)	3000/579	241/5-2.5	4.17/1.59	650/9.8	999/99
Slice thickness (mm)	0.6	5	1	3	5
FOV (mm <sup>2</sup> )	240 × 240	280 × 228	400 × 400	200 × 200	400 × 400
Acquisition time (min)	5	0.4	11	1.57	0.6
NEX	2	1	2	2	1
Slice number	240	35	224	15	26
Flip angle (°)	100°	70°	10°	150°	139°
Imaging plane	Sagittal	Axial	Coronal	Sagittal	Axial
Distance factor (%)	—	30	20	20	10
PAT factor	2	1	1	2	3
PAT mode	GRAPPA	—	—	GRAPPA	GRAPPA
Voxel size (mm <sup>3</sup> )	0.6 × 0.6 × 0.6	1.4 × 1.1 × 5	1 × 1 × 1	0.7 × 0.5 × 3	1.25 × .125 × 5
Fat-saturation	—	—	+	—	—

FOV, field of view; GRAPPA, generalized auto-calibrating partially parallel acquisitions; NEX, number of excitations; PAT, parallel acquisition technique; TR/TE, time of repetition/time of echo.

covered was 9.8% (the difference between theoretical loading and practical loading=0.2%).

### Water Content

The moisture content of the powder form of the LBXG mixture was found to be 1.8% in the moisture determination using the Karl Fischer method, and this ratio was reduced to 1.2% in the coated granules.

### Acid Resistance Test

In the acid resistance test, the viscosity values of the solution obtained when the coated granules were held for 1 hour at 37°C+0.5 at 20 rpm using a shaking water bath at pH 1.2 are shown in Table 2.

When the same experiments and conditions were repeated at pH 7.4, it was observed that the viscosity increased significantly and was close to the values in the uncoated powder of LBXG. The enteric coating can provide resistance to acidic environments in vitro.

### Particle Size and Distribution

The LBXG powder ranges from about 10-20 µm, while the coated granular LBXG ranges from 100 to 1000 µm (750 µm on average).

### Viscosity Values in Various Media

The uncoated and coated forms of the LBXG were dissolved in deionized water, pH 1.2, and pH 7.4; and their viscosities are given in Tables 2-4.

According to the tests, the viscosities increased depending on the amount of LBXG. The density values showed a linear increase depending on the concentration, although there was no significant difference in the order of pH 1.2 < water < pH 7.4 mediums. The results are shown in Figures 2-4. The enteric-coated LBXG mixture exhibited a minimum of 10 times water absorption in the intestinal environment (pH 4.5-7.4). It presented increased viscosity values depending on the application concentration (range: 0.5%-3%).



**Figure 1.** Uncoated powder (left images) and coated granular (right images) forms of the LBXG can be seen. The size of each square is 1000 µm in the upper images. The LBXG powder is in the range of about 10-20 µm, while the coated granular LBXG is in the range of 100-1000 µm (750 µm on average).

**Table 2.** Speed Per Minute (RPM), Torque (%), and Centipoise (cP) Values of Various Formulations of Uncoated Locust Bean and Xanthan Gums (LBXG, 1 : 1) Mixtures in Water

Formula	LBXG %	RPM	Torque %	cP
F1	0.5%	5	2.4	1320
		10	2.4	880
		20	3.0	540
		50	4.0	344
F2	1%	5	5.9	4080
		10	6.0	2400
		20	7.5	1520
		50	10.8	864
F3	2%	5	20.8	17300
		10	25.1	9280
		20	32.2	6200
		50	44.7	3560
F4	2.5%	5	14.5	16500
		10	18.9	8280
		20	24.2	5200
		50	35.7	2920
F5	3%	5	16.9	35000
		10	22.1	14800
		20	26.4	6600
		50	34.0	2960

**Table 3.** Speed Per Minute (RPM), Torque (%), and Centipoise (cP) Values of Various Concentrations of Uncoated LBXG (1 : 1) Mixtures in the Acidic Medium (pH 1.2)

Formula	LBXG %	RPM	Torque (%)	cP
F6	0.5%	5	0.70	400.00
		10	0.90	320.00
		20	1.20	220.00
		50	1.80	136.00
F7	1%	5	2.70	2480.00
		10	3.80	1520.00
		20	4.50	1020.00
		50	7.80	616.00
F8	2%	5	10.70	9040.00
		10	12.50	5640.00
		20	18.80	3760.00
		50	25.30	2160.00
F9	2.5%	5	22.50	18300.00
		10	25.60	11700.00
		20	37.90	7500.00
		50	50.80	4080.00
F10	3%	5	50.00	47600.00
		10	58.30	20500.00
		20	68.80	12100.00
		50	81.30	6440.00

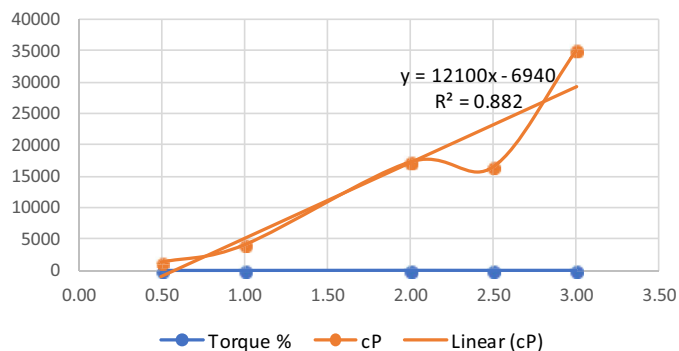
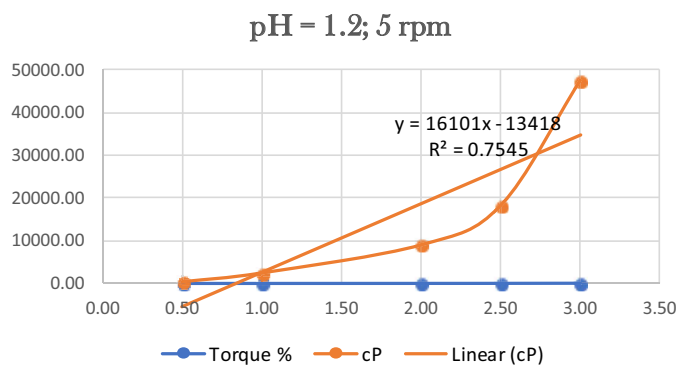
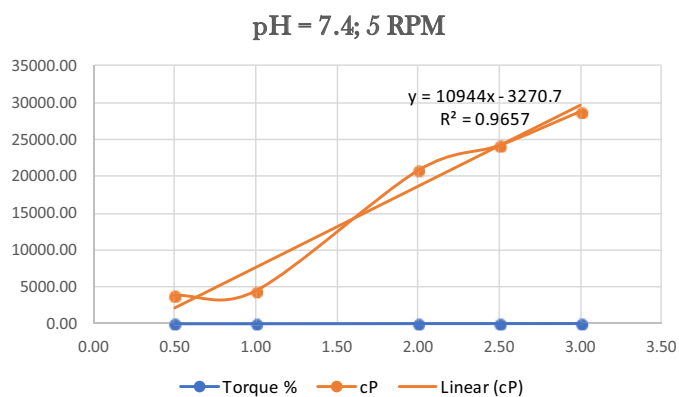
**Table 4.** Speed Per Minute (RPM), Torque (%), and Centipoise (cP) Values of Different Concentrations of the Uncoated Form of the LBXG (1 : 1) Mixture in the Phosphate Buffer (pH 7.4)

Formula	LBXG %	RPM	Torque %	cP
F11	0.5%	5	2.20	3680.00
		10	2.10	1520.00
		20	4.30	840.00
		50	5.70	464.00
F12	1%	5	4.40	4480.00
		10	5.20	2120.00
		20	6.30	1320.00
		50	9.20	776.00
F13	2%	5	23.50	20800.00
		10	29.60	12200.00
		20	41.60	8400.00
		50	62.00	4920.00
F14	2.5%	5	28.80	24200.00
		10	37.60	15100.00
		20	50.00	10100.00
		50	71.10	5720.00
F15	3%	5	33.50	28800.00
		10	36.70	16700.00
		20	42.90	8900.00
		50	53.00	4360.00

The viscosity values of enteric-coated LBXG (1 : 1) granules at a 1% concentration in different media are given in Table 5 and Figure 5.

### Computed Tomography and Magnetic Resonance Imaging Results

The average HU values of polyethylene glycol, lactulose, and carboxymethylcellulose solutions, as well as granule forms of LBXG in neutral, acidic, and basic environments, are given in Table 6. Among these, the lactulose-based solutions were hyperdense, whereas the others were isodense on CT images (Figure 6).

**Figure 2.** Viscosity graph of LBXG (1 : 1) mixture depending on its concentration in the water.**Figure 3.** Viscosity graph of LBXG (1 : 1) mixture depending on its concentration in the acidic environment (pH 1.2).**Figure 4.** Viscosity graph of LBXG (1 : 1) mixture depending on its concentration in the alkaline environment (pH 7.4).**Table 5.** Speed Per Minute (RPM), Centipoise (cP) Values of 1% Ratios of Coated Granules of LBXG Mixture (1 : 1) in the Water, pH 1.2, and pH 7.4

RPM	cP (water)	cP (pH 1.2)	cP (pH 7.4)
5	2025.00	810.00	4350.00
10	1210.00	475.00	2080.00
20	780.00	364.00	1276.00
50	432.00	226.00	760.00



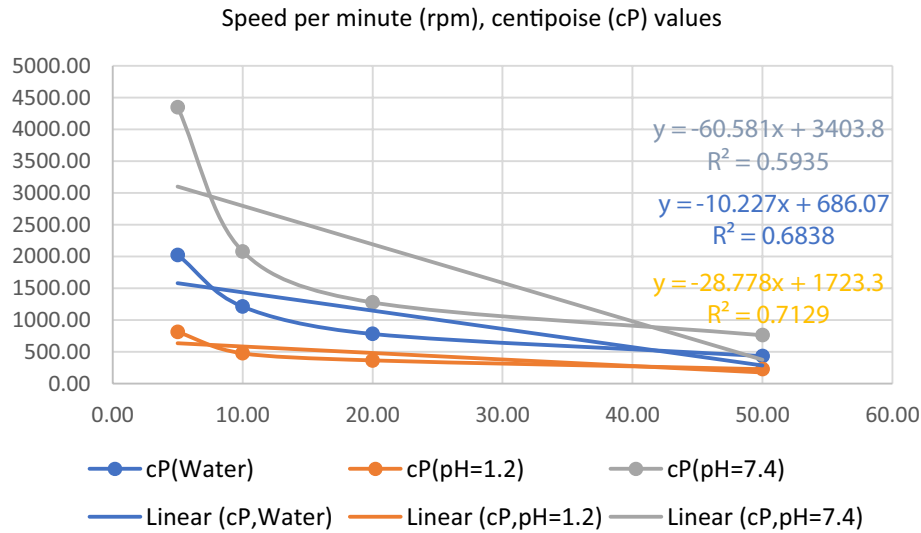


**Figure 5.** Graph of the viscosity values of a 1% solution of enteric-coated LBXG (1 : 1) in various media (deionized water, pH 1.2, and pH 7.4).

On CT and MR images, CMC-based solutions showed clumping in both water and acidic and basic environments despite sufficient shaking. This type of clumping was not observed in the other solutions. All oral contrast solutions were hypointense on T1-weighted images and hyperintense on T2-weighted MR images (Figure 7).

It was visually determined that the viscosity of the enteric-coated LBXG granules in water was lower than that of the enteric-coated LBXG granules in an alkaline medium. Although the enteric-coated LBXG was homogeneously soluble in water and an alkaline environment, it did

not dissolve and precipitated completely in an acidic solution despite sufficient shaking (Figure 7).

After LBXG administration, an increased distention was observed in the stomach and small bowels compared with pre-contrast images on MR images of the rabbit (Figure 8). Locust bean and xanthan gum was hypointense on T1-weighted images and hyperintense on T2-weighted MR images. Vomiting was not observed in rabbits after LBXG administration. After the MR examination, no unusual situation was observed except for diarrhea. The physical examination of the rabbit was normal during the first-week follow-up visit.

**Table 6.** Mean HU Values of the Oral Contrast Agents in Different Environments (PEG, polyethylene-glycol; CMC, carboxymethyl cellulose; LBXG, locust-bean and xanthan gums)

Solutions	Neutral	Acidic pH	Alkaline pH
	Mean (Range)	Mean (Range)	Mean (Range)
Lactulose	100 (94-102)	92 (87-95)	90 (87-92)
Polyethylene-glycol	17 (15-19)	18 (15-20)	26 (20-30)
CMC	6 (4-10)	12 (8-14)	20 (17-21)
LBXG	9 (6-13)	5 (2-7)	22 (19-27)

## DISCUSSION

The new enteric-coated oral contrast agent was described, and its effectiveness was investigated in this preliminary study. It has unique features for patients because of its bowel-specific nature. This natural oral contrast agent is resistant to the stomach environment and is more soluble at alkaline pH. This feature allows for more targeted dilatation of the small bowels. In addition, it would lead to a reduction in the incidence of side effects caused by stomach bloating. This will increase the patient's compliance and acceptability of the enteric-coated LBXG granules.

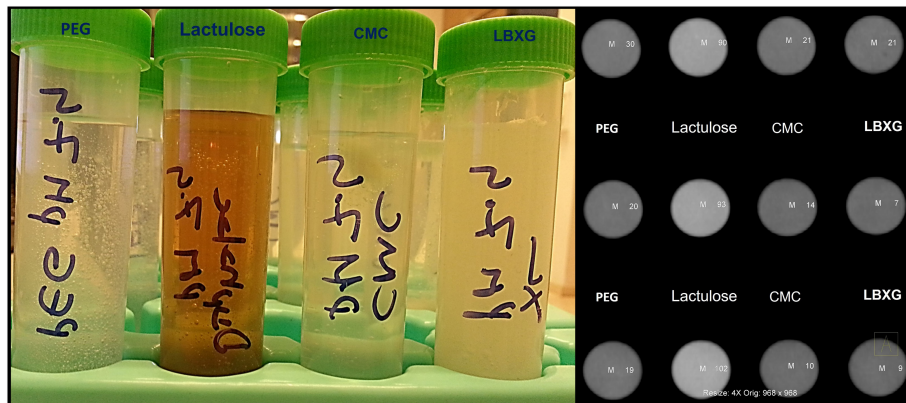


**Figure 6.** Mean Hounsfield units of commercially available oral contrast agent tubes [polyethylene-glycol (PEG), lactulose, carboxymethylcellulose (CMC)] for enterography and the enteric-coated LBXG granules on CT images. Lactulose-based solutions were hyperdense, while the others were isodense on CT images.

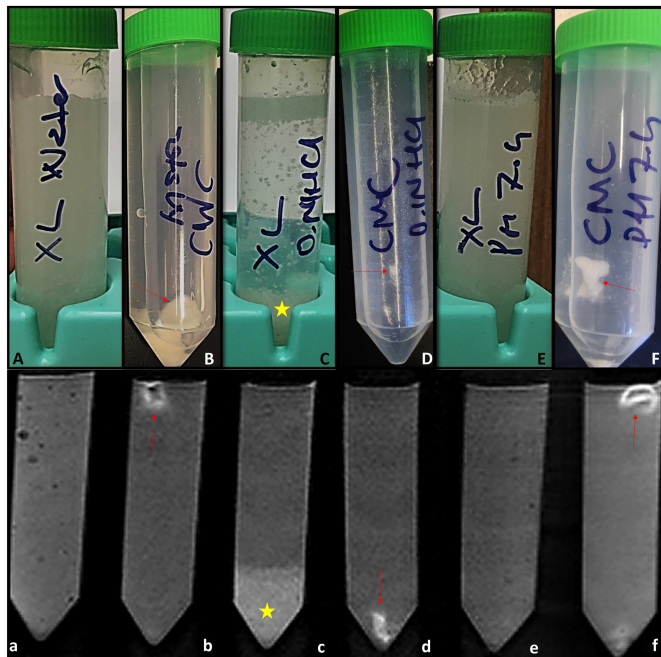


**Figure 7.** MR experiments of the oral contrast agents (lactulose and polyethylene glycol solutions are not shown here). Contrast agent-containing tubes were placed in a 32-channel head coil [upper line, LBXG in water (A-a), carboxymethyl cellulose in water (B-b), LBXG in an acidic environment (C-c), carboxymethyl cellulose in an acidic environment (D-d), LBXG in an alkaline environment (E-e), and CMC in an alkaline environment (F-f)]. There are many clumps in CMC solutions (arrows) on T1W MR images of the tubes (lower line). Also, a prominent aggregation was observed within the tube of the enteric-coated LBXG granules in the acidic buffer (asterisks).

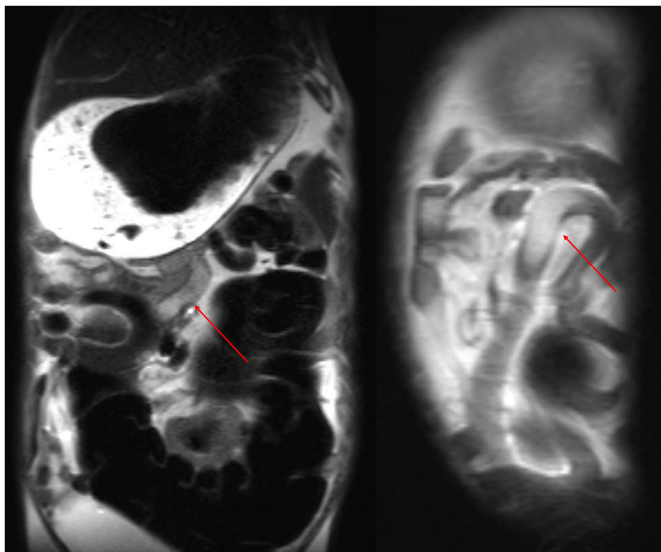


**Figure 8.** Coronal (left) and sagittal (right) planes T2-weighted MR images of the rabbit obtained after the LBXG administration. Small bowel dilatations were observed in these images (arrows).

Achieving proper expansion or filling of the small bowels is an essential requirement to achieve high sensitivity and specificity for detecting abnormalities on CT or MR enterography exams.<sup>1-5</sup> Recent advances in MRI technology have increased the role and success of

MR enterography in the evaluation of the gastrointestinal system.<sup>6</sup> Oral contrast materials used in MR enterography are classified as positive, negative, and biphasic agents.<sup>7</sup> The most preferred type is biphasic (hypointense on T1W and hyperintense on T2W MR images) agents, such as methylcellulose, PEG, sorbitol, lactulose, CMC, and mannitol.<sup>8</sup> In addition, these contrast agents are among the most preferred oral contrast agents in CT enterography.<sup>9</sup> Because of some of the disadvantages or side effects (e.g., diarrhea) of oral contrast agents, the question of which contrast agent is optimal for enterography exams remains unresolved.<sup>3,9</sup> The enteric-coated LBXG has a biphasic character on MR images and is hypodense on CT images, similar to the clinically popular oral contrast agents mentioned above.

Xanthan gum (E-415) is an important exopolysaccharide secreted by *Xanthomonas*, a gram-negative bacterium.<sup>10</sup> Locust bean gum (LBG) is an antioxidant galactomannan vegetable gum extracted from the seeds of the carob tree (*Ceratonia siliqua*) found mostly in the Mediterranean region.<sup>11</sup> Locust bean gum (E-410) has a lower caloric value and a higher viscosity in vitro than starches.<sup>12</sup> Locust bean gum also shows a synergistic increase in gel strength when blended with xanthan gum.<sup>13</sup> Xanthan and locust bean gums (LBXGs) are safe and are used as gelling and thickening agents in the food and drug industry.<sup>11</sup> They are soluble in water and have high viscosities at relatively low concentrations.<sup>10</sup> Locust bean and xanthan gums can regulate the intestinal microbial balance and colonic butyrate production.<sup>14</sup>

Locust bean gum is a natural antioxidant and viscous soluble fiber.<sup>13</sup> Therefore, it may improve mucosal integrity and contribute to the reduction of intestinal inflammation.<sup>14</sup> Locust bean gum has a hypolipidemic effect, decreasing low-density lipoprotein (LDL) because of its high dietary fiber content.<sup>13</sup> It also reduces or controls diabetes and obesity because of its high gelling ability, which on ingestion causes a satiety sensation.<sup>13</sup> Locust bean gum can be linked with polyphenols, which cause polyphenols to reach the colon, where they can act on the gastrointestinal tract, maintain intestinal health, and prevent colorectal cancer.<sup>15</sup>

Enteric-coated LBXG contains non-absorbable and herbal ingredients with a biodegradable coating. Therefore, it can be used as a food supplement that does not require drug-related phase tests or a drug license. Therefore, it may also be used as an anti-constipation agent, detox therapy, liquid thickener in treating dysphagia, and/or to reduce the frequency and volume of regurgitation.

Oral intake or toleration of LBXG will be more accessible when applied by mixing it with fruit juice or yogurt. In addition, this oral contrast agent has a lower production cost than its existing alternatives because it contains easily available herbal components. The LBXG has unique features such as biodegradability, eco-friendliness, bio-acceptability, and safety, and is derived from renewable sources.

Enteric-coated LBXG may not cause significant stomach swelling because of its acid-resistant nature. It may provide more effective intestinal distension with fewer side effects and good tolerance with its alkaline pH sensitivity. The properties of our new oral contrast media may allow fast, effective, and more tolerable enterography exams. In addition, it may act as a bowel cleaner before CT/MR imaging, surgery, or endoscopy.

Because LBXG is completely natural, it may be easily removed without accumulation in the patient's body. No unusual behavior or vomiting

was observed in rabbits after LBXG administration. It may have fewer side effects for the patients.

There are some limitations to this study. The animal experiment was conducted on one rabbit. Our animal experiment model, based on 5F-guiding neurocatheter usage, is the first to be reported in the literature. Our contrast media may cause some symptoms (e.g., abdominal bloating, pain, flatulence, nausea, borborygmi, and/or diarrhea) similar to those of unabsorbed carbohydrates (such as lactulose).<sup>16</sup> Because we had to administer the oral contrast agent with a nasogastric tube, we limited the number of animal experiments because animal experiments could not be an adequate simulation for humans. Comprehensive preliminary human studies of the efficacy and tolerability of the new oral contrast agent are required.

Our results showed that enteric-coated LBXG granules may be more effective, safe, and tolerable for enterography exams. It may provide better luminal distension than other biphasic contrast agents. Enteric-coated LBXG may also be used as an oral bowel cleanser, and it may reduce the incidence of side effects or toleration problems.

**Ethics Committee Approval:** Ethics committee approval was received for this study from the Ethics Committee of Veterinary Faculty, Ankara University (22nd August 2022, Number: 2022/16).

**Informed Consent:** N/A.

**Peer-review:** Externally peer-reviewed.

**Author Contributions:** Concept – O.A., M.O.; Design – O.A., C.O.; Supervision – O.A., M.O.; Resources – O.A., M.O.; Materials – O.A., M.O.; Data Collection and/or Processing – O.A., M.O.; Analysis and/or Interpretation – O.A., M.O.; Literature Search – O.A., C.O.; Writing Manuscript – O.A., M.O.; Critical Review – O.A., C.O.

**Declaration of Interests:** The authors have no conflict of interest to declare.

**Funding:** The authors declared that this study has received no financial support.

## REFERENCES

- Algin O, Turkbey B, Ozmen E, Algin E. Magnetic resonance enterography findings of chronic radiation enteritis. *Cancer Imaging*. 2011;11(1):189-194. [\[CrossRef\]](#)
- Evrimler Ş, Ocakoğlu G, Algin O. The efficacy of new oral contrast mixture for computed tomography enterography. *Pol J Radiol*. 2019;84:e403-e412. [\[CrossRef\]](#)
- Evrimler S, Algin O. MR enterography with oral contrast agent composed of methylcellulose, low-dose barium sulfate, sorbitol, and lactulose: assessment of diagnostic performance, reliability, image quality, and patient tolerance. *Clin Imaging*. 2016;40(3):523-530. [\[CrossRef\]](#)
- Algin O, Evrimler S, Ozmen E, et al. A novel biphasic oral contrast solution for enterographic studies. *J Comput Assist Tomogr*. 2013;37(1):65-74. [\[CrossRef\]](#)
- Algin O, Evrimler S, Arslan H. Advances in radiologic evaluation of small bowel diseases. *J Comput Assist Tomogr*. 2013;37(6):862-871. [\[CrossRef\]](#)
- Erol MY, Algin O. Detection of intramural fat accumulation by 3D-Dixon-Caipirinha-Vibe and the contribution of this technique to the determination of the chronicity of Chron's disease. *Magn Reson Imaging*. 2022;85:93-101. [\[CrossRef\]](#)
- Giovagnoni A, Fabbri A, Maccioni F. Oral contrast agents in MRI of the gastrointestinal tract. *Abdom Imaging*. 2002;27(4):367-375. [\[CrossRef\]](#)
- Riordan RD, Khonsari M, Jeffries J, Maskell GF, Cook PG. Pineapple juice as a negative oral contrast agent in magnetic resonance cholangiopancreatography: a preliminary evaluation. *Br J Radiol*. 2004;77(924):991-999. [\[CrossRef\]](#)
- Renosto FL, Barros JR, Bertoldi GA, Marrone SR, Sassaki LY, Saad-Hossne R. Comparative analysis of two oral contrast agent volumes for computed tomography enterography in Crohn's disease patients. *Arq Gastroenterol*. 2021;58(3):322-328. [\[CrossRef\]](#)
- Methacanon P, Gamonpilas C, Kongjaroen A, Buathongjan C. Food polysaccharides and roles of rheology and tribology in the rational design of thickened liquids for oropharyngeal dysphagia: a review. *Compr Rev Food Sci Food Saf*. 2021;20(4):4101-4119. [\[CrossRef\]](#)
- Alam MT, Parvez N, Sharma PK. FDA-approved natural polymers for fast dissolving tablets. *J Pharm (Cairo)*. 2014;2014:952970. [\[CrossRef\]](#)
- Bellaiche M, Ludwig T, Arciszewska M, et al. Safety and tolerance of a novel anti-regurgitation formula: a double-blind, randomized, controlled trial. *J Pediatr Gastroenterol Nutr*. 2021;73(5):579-585. [\[CrossRef\]](#)
- Barak S, Mudgil D. Locust bean gum: processing, properties and food applications--a review. *Int J Biol Macromol*. 2014;66:74-80. [\[CrossRef\]](#)
- Galvez J, Rodríguez-Cabezas ME, Zarzuelo A. Effects of dietary fiber on inflammatory bowel disease. *Mol Nutr Food Res*. 2005;49(6):601-608. [\[CrossRef\]](#)
- Zhu BJ, Zayed MZ, Zhu HX, Zhao J, Li SP. Functional polysaccharides of carob fruit: a review. *Chin Med*. 2019;14:40. [\[CrossRef\]](#)
- Montalto M, Gallo A, Ojetti V, Gasbarrini A. Fructose, trehalose and sorbitol malabsorption. *Eur Rev Med Pharmacol Sci*. 2013;17(suppl 2):26-29.

# Large Language Models on Magnetic Resonance Imaging Safety-Related Questions: Accuracy of ChatGPT-3.5, ChatGPT-4, Gemini, and Perplexity

Esat Kaba<sup>1</sup>, Hande Melike Bülbül<sup>1</sup>, Gülen Burakgazi<sup>1</sup>, Merve Solak<sup>1</sup>, Serdar Tabakoğlu<sup>1</sup>, Ayşenur Topçu Varlık<sup>1</sup>, Nur Hürsoy<sup>1</sup>, Fatma Beyazal Çeliker<sup>1</sup>

Department of Radiology, Recep Tayyip Erdogan University Faculty of Medicine, Rize, Turkey

**Cite this article as:** Kaba E, Bülbül HM, Burakgazi G, *et al.* Large language models on magnetic resonance imaging safety-related questions: accuracy of ChatGPT-3.5, ChatGPT-4, Gemini, and Perplexity. *Current Research in MRI* 2024;3(1):16-19.

**Corresponding author:** Esat Kaba, e-mail: esatkaba04@gmail.com

**Received:** March 13, 2024 **Revision requested:** April 3, 2024 **Last revision received:** April 4, 2024 **Accepted:** April 7, 2024 **Publication Date:** April 22, 2024

DOI:10.5152/CurrResMRI.2024.24095



Content of this journal is licensed under a Creative Commons Attribution-NonCommercial 4.0 International License.

## Abstract

**Objective:** This study investigates the accuracy of large language models (LLMs) on magnetic resonance imaging (MRI) safety-related questions.

**Methods:** Three experienced radiologists independently prepared 20 multiple-choice questions based on the MRI safety guidelines published by the Turkish Magnetic Resonance Society. An initial prompt was entered into 4 different LLMs (ChatGPT-3.5, ChatGPT-4, Gemini, and Perplexity) and then a total of 60 questions were asked. The answers received were compared with the answers assigned by the radiologists according to guidelines. The performance of each model was obtained as accuracy.

**Results:** In 60 questions, the accuracy rates were 78.3% (47/60) for ChatGPT-3.5, 93.3% (56/60) for ChatGPT-4, 88.3% (53/60) for Gemini, and 86.7% (52/60) for Perplexity. In addition, ChatGPT-3.5 answered 19/20, 13/20, and 15/20, ChatGPT-4 answered 18/20, 18/20, and 20/20, Gemini answered 19/20, 18/20, and 16/20, and Perplexity answered 20/20, 15/20, and 17/20 correctly to question groups prepared by 3 radiologists, respectively.

**Conclusion:** Large language models, particularly the most stable and highest performing ChatGPT-4, may be useful to patients and health-care professionals in providing MRI safety-related information. They have the potential to assist in the future to protect health-care professionals and patients from MRI-related accidents.

**Keywords:** Large language model, MRI safety, questions, accuracy

## INTRODUCTION

Large language models (LLMs) are a component of generative artificial intelligence (AI) that are trained with a lot of data and focus on the interaction between humans and computer language.<sup>1</sup> Such models are developed through unsupervised training where they learn the structures, patterns, and relationships of language by analyzing large amounts of textual data.<sup>2</sup> Training with a wide variety and size of data has significantly improved their ability to better understand human language and generate human-like text. After OpenAI launched ChatGPT in November 2022, it became very popular and reached millions of users quickly. Due to their high text analysis capabilities, their potential use in many fields of medicine is being explored.<sup>3</sup>

Potential uses of LLMs in radiology include topics such as radiology report generation, report structuring, report simplification, and radiological protocol determination.<sup>4</sup> In addition, studies testing the accuracy and reliability of LLMs' knowledge of radiology-related topics and evaluating their performance in creating patient educational materials have been published.<sup>5</sup> Patil et al<sup>6</sup> analyzed the answers to 318 questions in neuroradiology, general and physics, pediatric radiology, ultrasound, and nuclear medicine and compared the performance of ChatGPT and Bard. In this study, the accuracy rate of ChatGPT was remarkable at 87.11%. Large language models are also promising for facilitating patients' understanding of complicated radiologic terminology and providing summary reports to patients. One study investigated the accuracy of LLMs in summarizing full magnetic resonance imaging (MRI) reports of cancer patients and found satisfactory results.<sup>7</sup> However, as indicated in these studies, LLMs have some important limitations and much larger studies are needed to demonstrate the reliability of their potential use.<sup>6,7</sup>

Magnetic resonance imaging is a valuable technique in radiology due to its high soft tissue resolution and its absence of ionizing radiation, and its use is increasing worldwide.<sup>8</sup> It generates an electromagnetic force 30-60 thousand times stronger than the magnetic field strength of the earth.<sup>9</sup> This strong magnetic field can lead to fatal situations if safety rules are not followed.<sup>10</sup> Therefore, patients and health-care professionals must have adequate knowledge about MRI safety.



In this study, we tested the accuracy and reliability of LLMs on MRI safety to investigate their potential future usability by patients and health-care professionals.

## MATERIAL AND METHODS

In this study, 3 radiologists with 19, 14, and 8 years of radiology experience, respectively, independently prepared 20 multiple-choice questions (questions group 1, 2, and 3) related to MRI safety. All questions were based on the MRI safety guidelines of the Turkish Magnetic Resonance Society (TMRD) (<https://tmrd.org.tr/uploads/files/tmrd-m-r-klavuzu.pdf>). A total of 60 questions were created, and all questions were reviewed by another radiologist with 5 years of experience. Four sample questions and their options are shown in Table 1. Since no human or animal subjects were used, ethical approval or informed consent was not required.

The initial prompt was then entered into ChatGPT-3.5 and 4 (<https://chat.openai.com/>), Gemini, (<https://gemini.google.com/app>), and Perplexity (<https://www.perplexity.ai/>) chatbots. All questions were entered into 4 different language models with default parameters in March 2024. All questions and options are entered in English. Role-modeling technique was used in prompting. The initial prompt entered into the chatbots is as follows;

### Initial Prompt

“As a highly experienced radiologist with 25 years of experience, answer these questions about magnetic resonance imaging (MRI) safety, there is only one correct answer.”

The results were then analyzed and compared with the correct answers assigned by the radiologists according to guidelines. The flowchart of our study is shown in Figure 1.

## RESULTS

A total of 60 questions prepared by 3 radiologists were asked to 4 different LLMs. The accuracy rates were 78.3% (47/60) for ChatGPT 3.5, 93.3% (56/60) for ChatGPT-4, 88.3% (53/60) for Gemini, and 86.7% (52/60) for Perplexity. In other words, ChatGPT-4 performed the best compared to other LLM models, answering 56 out of 60 questions correctly.

ChatGPT-3.5 answered 19/20, 13/20, 15/20, ChatGPT-4 18/20, 18/20, 20/20, Gemini 19/20, 18/20, 16/20, and Perplexity 20/20, 15/20, 17/20 correctly to 3 radiologists' questions, respectively (Table 2).

The comparative graph of LLMs' answers to radiologist question groups is given in Figure 2.

## MAIN POINTS

- In this study, we analyzed the responses of large language models (LLMs) to magnetic resonance imaging (MRI) safety-related questions.
- ChatGPT-4 outperformed the other LLMs by answering 56 out of 60 multiple-choice questions correctly, with an accuracy of 93.3%.
- The accuracy rates of Gemini, Perplexity, and ChatGPT-3.5 are 88.3%, 86.7%, and 78.3%, respectively.
- Large language models can potentially assist patients and health-care professionals in MRI safety, as in many domains of radiology.

**Table 1.** Four Sample Questions

**1. Which of the following can cause strong gravitational or ejection effects (missile or projectile effect) and related injuries?**

- Static magnetic field
- Gradient magnetic field
- Radiofrequency energy

**2. In which MRI security zone is the MRI device located?**

- Zone 1
- Zone 2
- Zone 3
- Zone 4

**3. Which gas is discharged during the quench process in MRI?**

- Nitrogen
- Hydrogen
- Helium
- Oxygen

**4. Which of the implants and materials implanted in the human body is not classified as active in terms of MRI safety?**

- Aneurysm clips
- Pacemaker
- Implantable cardioverter defibrillator
- Neurostimulation system

MRI, magnetic resonance imaging.

The correct and incorrect answers of 4 different LLMs to a total of 60 questions are visualized in Figure 3.

## DISCUSSION

In this study, we investigated the accuracy of LLMs in MRI safety-related questions. Three different radiologists independently prepared a total of 60 questions based on the TMRD MRI safety guidelines. ChatGPT-3.5 and 4, Gemini, and Perplexity chatbots were used with default parameters. All questions were presented to LLMs with a role-modeling initial prompt technique. The answers were compared to the gold standard of correct answers. As a result, ChatGPT-4 showed the highest performance with 93.3% accuracy, answering 56 out of 60 questions correctly. ChatGPT-3.5 gave the correct answer to 47 out of 60 questions and showed the lowest performance with 78.3% accuracy. Gemini and Perplexity performed competitively with 88.3% and 86.7%, respectively.

In the field of natural language processing, LLMs, which are constantly making groundbreaking advances, are models for understanding, designing, reconstructing, and processing text.<sup>11</sup> Since November 2022, many companies have increasingly made continuously updated LLMs available to the general public. Although LLMs are trained for human-like speech, their perspective has broadened as the application has developed. Aiming to maximize productivity in health care and medical fields as in many industrial fields, these LLMs promise potential areas of use in radiology, which is directly affected by high technological developments. On the other hand, many radiology-based studies testing the accuracy and reliability of these LLMs, which have some concerns and limitations, have been published.<sup>12,13</sup>

Lee et al<sup>14</sup> investigated the accuracy of ChatGPT's answers to MRI-related questions.<sup>14</sup> In this study, the authors asked 50 simple MRI-related questions and categorized the answers as correct,

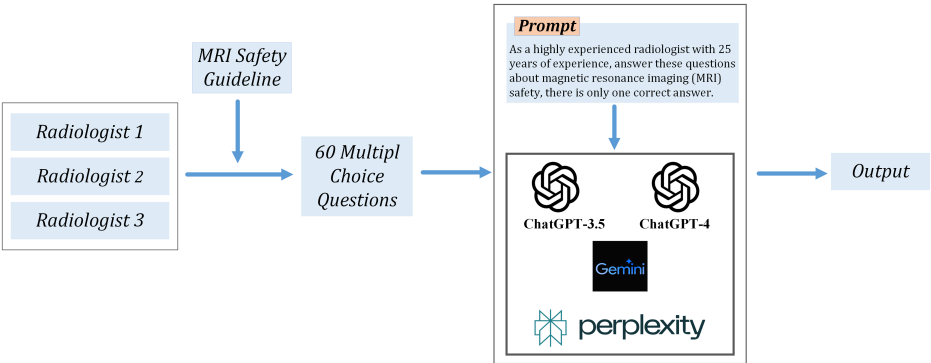


Figure 1. The flowchart of this study.

Table 2. Accuracy of Large Language Models

	Accuracy (Questions Group 1)	Accuracy (Questions Group 2)	Accuracy (Questions Group 3)	Accuracy (Total)
ChatGPT-3.5	95% (19/20)	65% (13/20)	75% (15/20)	78.3% (47/60)
ChatGPT-4	90% (18/20)	90% (18/20)	100% (20/20)	93.3% (56/60)
Gemini	95% (19/20)	90% (18/20)	80% (16/20)	88.3% (53/60)
Perplexity	100% (20/20)	75% (15/20)	85% (17/20)	86.7% (52/60)

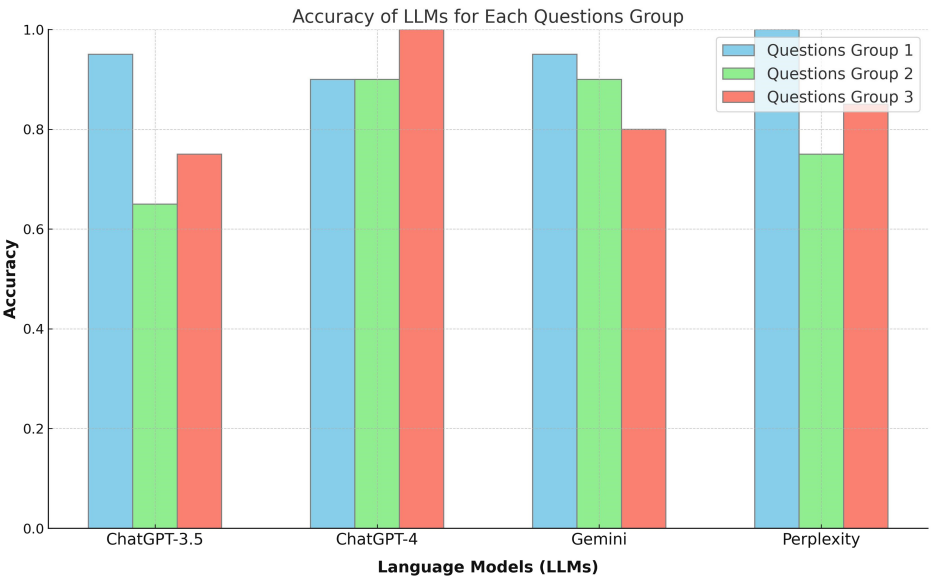
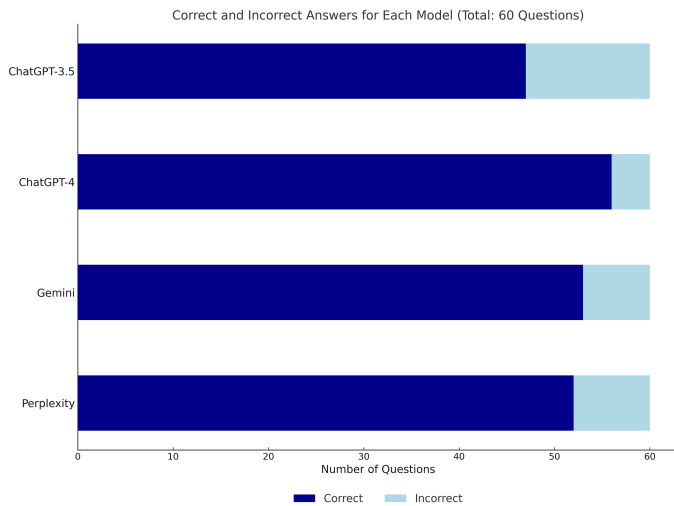


Figure 2. Comparative graph of large language models’ answers to radiologist question groups.

partially correct, and incorrect. In addition, they asked 75 multiple-choice questions on basic electromagnetism, MR magnets, gradients, radiofrequency and coils, and site planning, and the answers were analyzed by independent researchers. As a result, ChatGPT answered the 50 questions in the first step 86% and 88% correctly according to the 2 observers, respectively. The 75 multiple-choice questions in the second step were answered correctly between 40% and 66.7% depending on the topic. In our study, ChatGPT-3.5 answered 95%, 65%, and 75% correctly to the question groups prepared by 3 radiologists based on MR safety guidelines, respectively. ChatGPT-4 answered 90%, 90%, and 100% of the questions correctly, respectively. From this point of view, ChatGPT-4 is more successful and shows a more balanced accuracy value than the ChatGPT-3.5 version.

Magnetic resonance imaging is one of the most important radiology examinations without ionizing radiation and provides a high level of anatomical detail and functional imaging.<sup>15</sup> It has strong static and gradient magnetic fields and radiofrequency energy. The strong static magnetic field causes a ferromagnetic effect and when used inappropriately, metal materials in the patient’s body or the acquisition room can cause fatal injuries.<sup>16</sup> It also has the potential for many safety hazards, including tissue burns, nerve stimulation, acoustic noise, hearing loss, and contrast media complications.<sup>17</sup> There are also some rules to be considered for pregnant, children, and claustrophobic patients.<sup>18</sup> For all these reasons, radiologists, MRI technicians, and patients should have detailed information to prevent fatal errors. At this point, LLMs can benefit health-care professionals and patients regarding MRI safety in the future. If they can be securely integrated into hospital systems in



**Figure 3.** The correct and incorrect answers of 4 different large language models to a total of 60 questions.

the future, an application can be created that can detect the presence of any metal (e.g., pacemaker, aneurysm clip, orthopedic prosthesis) in the patient's body from the patient history and alert the technician. Thus, some potential errors that may occur under a heavy workload can be prevented. In addition, patients can access answers to their questions about MRI safety in a simplified way through LLMs. According to the results of our study, ChatGPT-4, which shows the highest performance with 93.3% accuracy, is promising for this purpose. However, LLMs, which have limitations such as timeliness problems, ethical concerns, confidentiality, bias, and hallucination generation, need much wider validation to be used in this field.<sup>19,20</sup>

There are several limitations of our study. First, the number of questions prepared was small. This is because the TMRD MRI safety guideline was used. This guideline is summarized. Large language models can be tested with a wider variety of questions than more comprehensive guidelines in the literature. Second, the questions were only prepared and entered into the LLMs in English. In the future, the performance of LLMs in different languages could be compared. Third, it should be noted that ChatGPT-4 is a paid LLM, and this may create limitations in its widespread use. Finally, the questions had a multiple-choice format with only 1 correct answer. In future larger studies, open-ended questions could be asked, and the answers provided by the LLMs could be analyzed by experienced radiologists.

In conclusion, although MRI is generally safe, it is a modality that can cause accidents with fatal consequences if several safety rules are not followed. Large language models can potentially provide information and decision support to radiologists, technicians, and patients on MRI safety, as in many areas of radiology. Furthermore, given the widespread use of LLMs in the community, they have the potential to increase the general population's level of knowledge about MRI safety.

**Ethics Committee Approval:** N/A.

**Informed Consent:** N/A.

**Peer-review:** Externally peer-reviewed.

**Author Contributions:** Concept – E.K., H.M.B., G.B., M.S., S.T., A.T.V., N.H., F.B.Ç.; Design – E.K., H.M.B., G.B., M.S.; Supervision – E.K., H.M.B.,

G.B., M.S., F.B.Ç.; Data Collection and/or Processing – E.K., H.M.B., G.B., M.S., S.T., A.T.V., N.H., F.B.Ç.; Materials – E.K., H.M.B., G.B., M.S., S.T., A.T.V., N.H., F.B.Ç.; Analysis and/or Interpretation – E.K., H.M.B., G.B., M.S., S.T., A.T.V., N.H., F.B.Ç.; Literature Search – E.K., H.M.B., G.B., M.S., S.T., A.T.V., N.H., F.B.Ç.; Writing Manuscript – E.K., H.M.B., G.B., M.S., S.T., A.T.V., N.H., F.B.Ç. Critical Review – E.K., H.M.B., G.B., M.S., S.T., A.T.V., N.H., F.B.Ç.

**Declaration of Interests:** The authors have no conflict of interest to declare.

**Funding:** The authors declared that this study has received no financial support.

## REFERENCES

- Cascella M, Semeraro F, Montomoli J, Bellini V, Piazza O, Bignami E. The breakthrough of large language models release for medical applications: 1-year timeline and perspectives. *J Med Syst.* 2024;48(1):22. [\[CrossRef\]](#)
- Birhanie A, Kasirzadeh A, Leslie D, Wachter S. Science in the age of large language models. *Nat Rev Phys.* 2023;5(5):277-280. [\[CrossRef\]](#)
- Abd-Alrazaq A, AlSaad R, Alhuwail D, et al. Large language models in medical education: opportunities, challenges, and future directions. *JMIR Med Educ.* 2023;9:e48291. [\[CrossRef\]](#)
- Kim S, Lee CK, Kim SS. Large language models: A guide for radiologists. *Korean J Radiol.* 2024;25(2):126-133. [\[CrossRef\]](#)
- Gordon EB, Towbin AJ, Wingrove P, et al. Enhancing patient communication with chat-GPT in radiology: evaluating the efficacy and readability of answers to common imaging-related questions. *J Am Coll Radiol.* 2024;21(2):353-359. [\[CrossRef\]](#)
- Patil NS, Huang RS, van der Pol CB, Larocque N. Comparative performance of ChatGPT and Bard in a text-based radiology knowledge assessment. *Can Assoc Radiol J.* 2023;8465371231193716. [\[CrossRef\]](#)
- Chung EM, Zhang SC, Nguyen AT, Atkins KM, Sandler HM, Kamrava M. Feasibility and acceptability of ChatGPT generated radiology report summaries for cancer patients. *Digit Health.* 2023;9:20552076231221620. [\[CrossRef\]](#)
- Sammet S. Magnetic resonance safety. *Abdom Radiol (NY).* 2016;41(3):444-451. [\[CrossRef\]](#)
- Panych LP, Madore B. The physics of MRI safety. *J Magn Reson Imaging.* 2018;47(1):28-43. [\[CrossRef\]](#)
- Dempsey MF, Condon B, Hadley DM. MRI safety review. *Semin Ultrasound CT MR.* 2002;23(5):392-401. [\[CrossRef\]](#)
- Cascella M, Semeraro F, Montomoli J, Bellini V, Piazza O, Bignami E. The Breakthrough of Large Language Models Release for Medical Applications: 1-Year Timeline and Perspectives. *J Med Syst.* 2024 Feb 17;48(1):22. doi: [\[CrossRef\]](#)
- Sun Z, Ong H, Kennedy P, et al. Evaluating GPT4 on impressions generation in radiology reports. *Radiology.* 2023;307(5):e231259. [\[CrossRef\]](#)
- Kaba E. Zero-, Single-, and Few-Shot Learning in Large language models to identify incidental findings from radiology reports. In: *AJR Am J Roentgenol.* 2024;1. [\[CrossRef\]](#)
- Lee KH, Lee RW. ChatGPT's accuracy on magnetic resonance imaging basics: characteristics and limitations depending on the question type. *Diagnostics (Basel).* 2024;14(2):171. [\[CrossRef\]](#)
- Starekova J, Hernando D, Pickhardt PJ, Reeder SB. Quantification of liver fat content with CT and MRI: state of the art. *Radiology.* 2021;301(2):250-262. [\[CrossRef\]](#)
- Tsai LL, Grant AK, Morteale KJ, Kung JW, Smith MP. A practical guide to MR imaging safety: what radiologists need to know. *RadioGraphics.* 2015;35(6):1722-1737. [\[CrossRef\]](#)
- Cross NM, Hoff MN, Kanal KM. Avoiding MRI-related accidents: A practical approach to implementing MR safety. *J Am Coll Radiol.* 2018;15(12):1738-1744. [\[CrossRef\]](#)
- Expert Panel on MR Safety, Kanal E, Barkovich AJ, et al. ACR guidance document on MR safe practices: 2013. *J Magn Reson Imaging.* 2013;37(3):501-530. [\[CrossRef\]](#)
- Sallam M, Chat GPT. ChatGPT Utility in healthcare education, research, and practice: systematic review on the promising perspectives and valid concerns. *Healthcare (Basel).* 2023;11(6):887. [\[CrossRef\]](#)
- Ullah E, Parwani A, Baig MM, Singh R. Challenges and barriers of using large language models (LLM) such as ChatGPT for diagnostic medicine with a focus on digital pathology- a recent scoping review. *Diagn Pathol.* 2024;19(1):43. [\[CrossRef\]](#)

# Advances in Machine Learning for Magnetic Resonance Imaging of Acute Ischemic Stroke: A Systematic Review

Sena Azamat<sup>1,2</sup> , Erdem Gürkaş<sup>1,3</sup> , Esin Ozturk-Isik<sup>1</sup> 

<sup>1</sup>Institute of Biomedical Engineering, Bogazici University, Istanbul, Turkey

<sup>2</sup>Department of Radiology, Basaksehir Cam and Sakura City Hospital, Istanbul, Turkey

<sup>3</sup>Department of Neurology, Kartal Lutfi Kırdar City Hospital, Istanbul, Turkey

**Cite this article as:** Azamat S, Gürkaş E, Ozturk-Isik E. Advances in machine learning for magnetic resonance imaging of acute ischemic stroke: A systematic review. *Current Research in MRI*, 2024;3(1):20-26.

**Corresponding author:** Esin Ozturk Isik, e-mail: esin.ozturk@bogazici.edu.tr

**Received:** November 20, 2023 **Revision Requested:** January 21, 2024 **Last Revision Received:** February 19, 2024 **Accepted:** February 27, 2024

**Publication Date:** April 22, 2024

DOI:10.5152/CurrResMRI.2024.23085



Content of this journal is licensed under a Creative Commons Attribution-NonCommercial 4.0 International License.

## Abstract

Stroke demands rapid and precise diagnosis. Recent advancements in machine learning (ML) have facilitated its integration with magnetic resonance imaging (MRI) for assessing acute ischemic stroke (AIS). This systematic review delves into the utilization of ML algorithms in MRI-based AIS diagnosis and prediction, highlighting their prospective clinical implementation.

This systematic review followed PRISMA guidelines, conducting a thorough search across PubMed, Web of Science, Scopus, and Google Scholar. Inclusion criteria focused on studies predicting acute stroke onset time and identifying acute ischemic stroke within the therapeutic window using MRI data for AI algorithms. Only studies post January 1, 2018, were included. Excluded were studies involving chronic stroke patients, computed tomography (CT) scans, other imaging modalities, or lacking AI components.

Twelve articles met the criteria, primarily aiming to predict tissue status or ischemic core using deep learning techniques like CNNs, U-Nets, autoencoders, and GANs, often with attention mechanisms or pretrained networks. Magnetic resonance imaging modalities included ADC, DWI, FLAIR, and T2W, with some using advanced techniques like PWI and pCASL. Model performances varied, with some achieving high accuracy in identifying patients within treatment windows and segmenting ischemic regions. One study generated synthetic MRI data, while another accelerated MRI acquisition.

Machine learning algorithms exhibit promise in MRI-based AIS diagnosis and prediction, especially in segmenting ischemic regions and classifying patients for treatment. However, validation on larger and diverse cohorts is essential for robustness. Integrating ML techniques into MRI protocols could enhance AIS diagnosis and treatment planning efficiency and accuracy in the future.

**Keywords:** Machine learning, MRI, stroke

## INTRODUCTION

Stroke is a serious health issue that has significant impacts on individuals, communities, and economies worldwide.<sup>1</sup> It results in disabilities and death, and it also imposes a substantial economic burden, with estimated costs reaching approximately 34 billion dollars each year.<sup>2,3</sup> There are 2 primary types of stroke, which are ischemic stroke and hemorrhagic stroke. Ischemic stroke is the more common type, accounting for approximately 87% of all stroke cases. Ischemic stroke occurs when there is a blockage or clot in a blood vessel that supplies blood to the brain, leading to a lack of oxygen and nutrients, and ultimately causing damage to the brain tissue. Hemorrhagic stroke, on the other hand, occurs when there is bleeding in the brain due to a ruptured blood vessel. Both types of stroke can have severe consequences and require prompt medical attention.<sup>3</sup> During an acute ischemic stroke (AIS), there are 2 distinct areas of the brain that are affected: the penumbra and the infarction core. The penumbra is a region surrounding the infarction core that is considered reversible, meaning that brain cells in this area can still recover if blood flow is restored promptly. The infarction core, on the other hand, is an irreversible ischemic area, where brain cells have already been damaged due to the lack of oxygen and nutrients. The American Heart Association/American Stroke Association (AHA/ASA) recommends 2 primary treatment options for restoring blood flow in AIS, which are thrombolysis with tissue plasminogen activator (tPA) administered either intra-arterially or intravenously, and mechanical thrombectomy, also known as clot retraction.<sup>4</sup> Mechanical thrombectomy is considered the gold standard for the treatment of large vessel occlusions in acute ischemic stroke.<sup>5</sup> However, both tPA thrombolysis and mechanical thrombectomy are time-sensitive procedures that are typically performed within specific time windows after the onset of stroke. Tissue plasminogen activator thrombolysis is usually done within 4.5 hours from the onset of stroke, while mechanical thrombectomy is typically performed within 6 hours from the onset of stroke.<sup>6</sup> The importance of timely intervention in acute ischemic stroke cannot be overstated, as theoretical calculations suggest that every 1.6 minutes saved from the onset time of stroke could potentially spare approximately 3.1 million neurons from damage or death, leading to improved outcomes.<sup>7</sup> Recent prospective randomized studies, such as the DAWN study<sup>8</sup> and the DEFUSE-3<sup>5</sup> study, have expanded the treatment window for endovascular intervention in acute ischemic stroke cases, with the DAWN study showing that intervention can be extended up to 24 hours from the onset of stroke, and



the DEFUSE-3 study demonstrating the safety of intervention up to 16 hours.<sup>5,9,10</sup>

One challenge in treating AIS is determining the exact time of stroke onset, particularly for patients who experience a stroke during their sleep or unwitnessed strokes, known as wake-up stroke (WUS), which accounts for a significant portion of acute ischemic stroke cases.<sup>11</sup> Wake-up stroke patients have traditionally been excluded from treatment due to the inability to accurately ascertain the time of stroke onset. However, the “Wake Up Trial,” conducted in 2018, was a groundbreaking study that challenged the traditional time-based approach for AIS treatment for intravenous thrombolysis. The study enrolled 503 patients who had an AIS with an unknown time of onset. Instead of relying solely on the time-based approach, the “Wake Up Trial” used advanced MRI imaging features, including the mismatch between diffusion-weighted imaging (DWI) and fluid-attenuated inversion recovery (FLAIR) in the region of ischemia, to guide thrombolysis treatment decisions. Diffusion-weighted imaging is a sensitive imaging technique that can detect early changes in brain tissue affected by ischemia, while FLAIR is a sequence that can help identify the presence of older, established infarcts.<sup>12</sup> The results of the “Wake Up Trial” showed that thrombolysis treatment guided by MRI features led to better outcomes compared to a control group that did not receive thrombolysis. Patients who received thrombolysis based on MRI findings had improved functional outcomes and higher rates of functional independence at 90 days compared to the control group.<sup>13,14</sup> Based on these findings, the most recent guidelines from the AHA recommend using MRI to evaluate the suitability of interventions in the WUS population.<sup>4</sup> However, evaluating this mismatch can be subject to significant variability when multiple readings or radiologists are involved.<sup>15</sup> Furthermore, typical MRI stroke protocols may take 10-15 minutes to perform, even with the advanced rapid protocols. Acute ischemic stroke imaging with MRI creates a mean delay of 18 minutes in workflow when compared to computed tomography (CT) scanning.<sup>16,17</sup> It is important to note that reducing the intervention time by even 15 minutes to restore blood flow can potentially lead to improved outcomes with reduced disability for a significant number of patients.<sup>18</sup> To identify relevant imaging findings in WUS patients efficiently and accurately can save time and standardize evaluation. Despite ongoing efforts to optimize stroke imaging, there is still a lack of timely and consistent stroke detection and triage methods that can be implemented immediately and in a standardized manner.

Machine learning (ML) has recently gained popularity and been used for many medical image acquisition and analysis procedures, including acquiring and reconstructing fast MR imaging data,<sup>19</sup> segmenting lesions on MR images,<sup>20</sup> classification of disease characteristics based on MRI,<sup>21</sup> and increasing the image spatial resolution.<sup>22</sup> Several studies have been reported for the use of machine learning algorithms in imaging WUS patients.<sup>23-25</sup> The main attempt of these studies is to enhance clinical outcomes by minimizing treatment delays, even if it is only by a few minutes. Machine learning algorithms are already extensively employed in patient triage for AIS treatments using computed tomography (CT).<sup>26</sup> Multiple studies have shown that automated approach based on CT is non-inferior to assessments made by experienced neuroradiologists.<sup>27-29</sup>

This systematic review aims to provide a comprehensive overview of recent advancements in utilizing ML algorithms for imaging AIS patients with MRI, with a particular emphasis on their potential implementation in clinical practice. By synthesizing current evidence and

highlighting emerging trends, this review aims to elucidate the evolving landscape of AIS imaging and the transformative role ML may play in enhancing diagnostic accuracy, prognostication, and patient management strategies. Ultimately, the integration of ML-driven MRI analysis into routine stroke care pathways has the potential to revolutionize the field, enabling more precise and personalized approaches to AIS diagnosis and treatment.

## METHODS

This systematic review followed the Preferred Reporting Items for Systematic Reviews and Meta-Analyses (PRISMA) guidelines and conducted a search on PubMed, Web of Science, Scopus, and Google Scholar specifically targeting peer-reviewed articles in English. The predetermined search terms included “artificial intelligence,” “machine learning,” or “deep learning,” in combination with “acute ischemic stroke,” “magnetic resonance imaging,” “acute ischemic stroke onset time,” or “treatment time window.” The inclusion criteria encompassed studies that focused on predicting acute stroke onset time using magnetic resonance imaging (MRI) or identifying AIS within the therapeutic time window using MRI, and included wake-up stroke and acute stroke patients. Additionally, the studies that utilized raw MRI data as input for artificial intelligence algorithms and published after January 1, 2018, were selected. Studies involving chronic stroke patients, computed tomography, other imaging modalities, or lacking artificial intelligence were excluded from the review. Figure 1 demonstrates an AIS patient who had the progression of ischemic stroke from the acute phase (within 6 hours) to the acute-subacute stage (beyond 6 hours) in the M1 segment of the middle cerebral artery.

## RESULTS

A total of 12 papers met all inclusion and exclusion criteria. The summary of these studies is given in Table 1.

The majority of studies aimed to predict tissue at risk and the ischemic core using artificial intelligence. However, there were 2 exceptions. One study conducted by Benzakoun et al<sup>19</sup> primarily focused on the generation of synthetic data, and another conducted by Verclytte et al.<sup>30</sup> focused on accelerating image acquisition. All the mentioned studies had cohorts larger than 100 patients except the study conducted by Qun-Zhang.<sup>23</sup> Furthermore, the majority of MR images used in these studies were acquired on 1.5 T or 3T scanners.

Zhu et al<sup>31</sup> conducted a study aiming to segment the ischemic core in DWI and FLAIR images and classify lesions based on the onset time of stroke. The study utilized a multi-institutional cohort, and all images were acquired using a 3T clinical MR scanner. In this study, an automatic machine learning method was proposed to classify time since stroke (TSS) as less than or more than 4.5 hours. A cross-modal convolutional neural network (CNN) was developed to achieve accurate segmentation of stroke lesions from DWI and FLAIR images. For the segmentation tasks, 5 different EfficientNet-B0 based U-Net algorithms were employed.<sup>32</sup> Subsequently, some features were extracted from the DWI and FLAIR images based on the segmented regions of interest (ROI) using Pyradiomics.<sup>33</sup> Finally, these extracted features were provided as inputs into machine learning models to identify the TSS. Evaluation metrics such as Dice similarity coefficient, sensitivity, specificity, and accuracy were used to assess the performance of the proposed model. Remarkably, the model achieved relatively high sensitivity and specificity, both exceeding 0.80, in identifying patients who had less than 4.5 hours since the onset of a stroke.

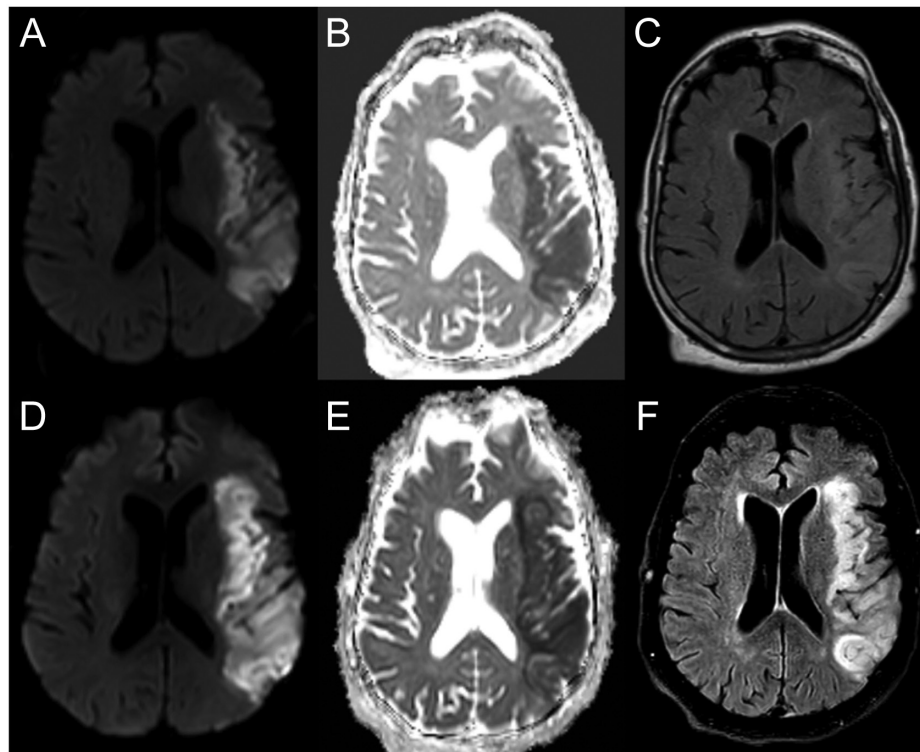


**Figure 1.** The images demonstrate the progression of ischemic stroke from the acute phase (within 6 hours) to the acute–subacute stage (beyond 6 hours) in the M1 segment of the middle cerebral artery. A–C, acute ischemic stroke within 6 hours; D–F, acute–subacute stage of ischemic stroke beyond 6 hours. A and D, DWI with b-value of  $1000 \times 10^{-6} \text{ s/mm}^2$ ; B and E, ADC map; C and F, FLAIR image.

In addition, Ho and colleagues conducted studies in 2018<sup>34</sup> and 2019<sup>24</sup> focusing on determining stroke time onset utilizing MRI through the application of deep learning, with a specific emphasis on autoencoders. Although these studies were innovative, they had the drawback of utilizing only their institutional cohort for analysis. The studies utilized MRI images acquired on 1.5 and 3 T clinical scanners. The imaging modalities included DWI, Apparent Diffusion Coefficient (ADC), Perfusion-Weighted Imaging (PWI), and FLAIR. Perfusion-weighted imaging images were used to generate perfusion parameters such as mean transit time (MTT), time to peak (TTP), cerebral blood volume (CBV), cerebral blood flow (CBF), and time to maximum (Tmax). A threshold of Tmax > 6 seconds was employed for segmentation of the ROIs. In the 2018 study, baseline features were extracted by determining the mean intensity values of the images at ROIs. Deep learning algorithms based on autoencoders were then used to extract hidden PWI features. Both baseline and hidden features were utilized to devise machine learning algorithms. The classification task, aimed at identifying a TSS of less than 4.5 hours using only baseline features, achieved an area under the curve (AUC) of 0.57. However, the inclusion of both baseline and deep features enhanced the classification task, elevating the AUC to 0.68.<sup>34</sup> In a subsequent study in 2019, the same group enriched the extraction of baseline features by incorporating additional descriptive features, namely mean, median, skewness, and kurtosis, while maintaining the deep learning aspect of the study intact. The combination of autoencoder-based deep features and baseline features achieved the best performance in predicting TSS of less than 4.5 hours, with an AUC of 0.76.<sup>24</sup>

In 2020, Yu et al.<sup>35</sup> embarked on a study aimed at predicting the final ischemic core, an area of permanent tissue damage following a stroke, using baseline MRI and deep learning techniques. This study

brought together 182 patients from 2 separate cohorts across different institutions. The patients underwent clinical MR scans at 1.5 T and 3 T, employing various imaging modalities, including DWI, PWI, T2-weighted MRI (T2W), and FLAIR. The team used PWI to obtain perfusion parameter maps and established tissue-at-risk parameters based on a Tmax exceeding 6 seconds, while identifying the ischemic core with an ADC below  $620 \times 10^{-6} \text{ mm}^2/\text{s}$ . The “ground truth” data, or verified data used for comparison with predictions, was sourced from T2W-MRI and FLAIR scans taken 3–7 days post stroke. A deep learning model utilizing an attention-gated U-Net, which incorporated consecutive slices of various imaging data and masks of Tmax and ADC, achieved a median AUC of 0.92 in identifying the final infarction without accounting for any subsequent reperfusion in the patients. Similarly, in 2021, the same researchers aimed to estimate tissue at risk and the ischemic core using the same deep learning approach.<sup>36</sup> This study exhibited superiority compared to the former study in terms of including more patients from 3 prospective multicenter stroke trials. The MR images were acquired at 1.5 T and 3 T MRI scanners, employing the same imaging modalities as the previous study. An attention-gated U-Net, with an identical architecture to the aforementioned study, was utilized. It incorporated 5 consecutive slices of DWI, ADC, Tmax, MTT, CBF, and CBV images, along with masks of Tmax and ADC, as inputs. The key difference between these 2 studies centered on considering the patient’s reperfusion status during the training phase. This status was categorized into minimal (20%), partial (20%–80%), and major (80%) reperfusion, determined based on a 4–24-hour follow-up PWI. The segmentation task utilizing the attention-gated U-Net outperformed the thresholding method that relied on DWI/PWI thresholds. The proposed deep learning method achieved an AUC of 0.97 for predicting the ischemic core.

**Table 1.** Summary of MRI of Ischemic Stroke Studies Utilizing Artificial Intelligence

Study	Number of Patients	MRI Scanner Field Strength	AI Tasks	MRI Sequences	AI Methods	Conclusion
Zhu et al <sup>31</sup>	268	3 T	Segmentation and classification	FLAIR and DWI	Deep CNN (U-Net) for segmentation, feature extraction by Pyradiomics, and ML for classification	Segmentation task dice score for FLAIR <0.80, dice score for DWI >0.80, classification task with ML using features extracted from manual labeling and segmentation ROI are around 0.80.
Chung Ho et al <sup>24</sup>	181	1.5 and 3 T	Classification	PWI, FLAIR, DWI, and ADC	Deep feature maps were extracted from PWI by deep autoencoder. ML classification was used for morphological and descriptive features including mean, median, etc. The total number of baseline features=104, deep features=384	Classification task with ML achieved an AUC of 0.76 using perfusion parameters map + deep features
Chung Ho et al <sup>34</sup>	105	1.5 and 3 T	Classification	PWI, DWI, FLAIR and ADC	Deep feature maps were extracted from PWI by deep autoencoder. ML classification was used for the intensity value of perfusion parameter maps, DWI, FLAIR and ADC. The total number of baseline features=7	Classification tasks with ML achieved an AUC of 0.57 using baseline features. The classification task with ML achieved an AUC of 0.68 using baseline and deep features
Yu et al <sup>36</sup>	237	1.5 and 3 T	Segmentation	DWI, ADC, Tmax, MTT, CBV, CBF	Attention-gated U-Net was used for segmentation tasks. Tmax>6 seconds was used to define tissue at risk and ADC<620 × 10 <sup>-6</sup> mm <sup>2</sup> /s for ischemic core. T2 and FLAIR acquired at 3-7 days were used as ground truth.	Segmentation task with attention-gated U-Net outperformed thresholding method which uses DWI/PWI thresholds. The proposed deep learning method achieves 0.97 AUC to predict ischemic core.
Do et al. <sup>37</sup>	390	1.5 T	Classification	DWI	ASPECT score prediction with recurrent residual convolutional neural network	Proposed model RRCNN outperformed the pre-trained CNN with accuracy of 87.3
Nazari-Farsani et al <sup>38</sup>	445	1.5 and 3 T	Segmentation	DWI, ADC, and thresholded ADC as input and T2-FLAIR and DWI for ground truth	Attention gated U-Net is used for delineation ischemic core.	The DCNN model predicted the final stroke lesions significantly better than the simple ADC thresholding method with AUC of 0.91 with dice similarity coefficient threshold of 0.50
Benzakoun et al <sup>19</sup>	1416	1.5 T	Synthetic data generation	DWI and FLAIR	Generative adversarial network was used for generation of synthetic FLAIR from DWI images.	Synthetic FLAIR had diagnostic performances similar to real FLAIR in depicting DWI-FLAIR mismatch
Verclytte et al <sup>30</sup>	173	3 T	MR reconstruction	T2W, T2W*, FLAIR, and DWI	Deep learning methods were used for acceleration of acquisition	The study highlights the high performance and reproducibility of the ultrafast MRI protocol in the acute ischemic stroke assessment
Wang et al <sup>39</sup>	137	1.5 and 3 T	Segmentation	pCASL, ADC, and Tmax	High-resolution 3Dnet were trained by ASL, Tmax, and ADC. PWI images were used for ground truth.	The study trained DL models with an input of noncontrast ASL images, using the hypoperfusion lesion observed on DSC MRI as the label. The model achieved an accuracy of 0.92 for image-based decision.
Yu et al <sup>35</sup>	182	1.5 and 3 Te	Segmentation	DWI, ADC, Tmax, MTT, CBV, CBF	Attention-gated U-Net was used for segmentation tasks. Tmax>6 sec was used to define tissue at risk and ADC<620 × 10 <sup>-6</sup> mm <sup>2</sup> /s for ischemic core. T2WI and FLAIR acquired at 3-7 days were used as ground truth.	Segmentation task with attention-gated U-Net outperformed thresholding method which uses DWI/PWI thresholds. Deep learning methods achieved moderate to excellent segmentation tasks for both ischemic core and tissue at risk.
Zhang et al <sup>25</sup>	422	1.5 and 3 T	Classification	T2W, DWI, and FLAIR	Attention-gated pre-trained weights were used for feature extraction and classification in a single slice. Attention-gated 3D U-Net and CNN from scratch was used for feature extraction and classification.	The pretrained 2D model achieved the highest performance metrics with a sensitivity of 0.70 and a specificity of 0.81 in classifying TSS < 4.5 hours.
Zhang et al <sup>23</sup>	84	3 T	Classification	ADC, DWI, and T1W	Radiomics features were used for feature extraction. ML and DL were used for classification.	DL model achieved the highest performance with an accuracy of 0.72 than conventional ML methods.

Furthermore, Do et al<sup>37</sup> conducted a study with the aim of classifying DWI images based on Alberta Stroke Program Early CT Score (ASPECTS) using deep learning algorithms. The study included 390 DWI scans acquired on a 1.5 T MRI scanner. The researchers developed a classifier algorithm to differentiate between low (1-6) and high (7-10) DWI-ASPECTS groups. Two different deep learning algorithms were compared in the study, a recurrent residual convolutional neural network (RRCNN) and a pre-trained 3D CNN, as well as a 3D CNN trained from scratch. The performance of these algorithms was evaluated and compared. The researchers concluded that the proposed model based on RRCNN outperformed both the pre-trained 3D CNN and the 3D CNN trained from scratch. The RRCNN achieved an accuracy of 0.87 in the classification task, demonstrating its superior performance in distinguishing between low and high DWI-ASPECTS groups.

Additionally, Nazari-Farsani et al<sup>38</sup> conducted a study aiming to predict the final ischemic core from baseline DWI data using deep learning. The strength of this study lies in its patient cohort, which consisted of 445 patients recruited from multiple institutions. The ground truth for the final ischemic core was determined using T2W and FLAIR scans taken 3-7 days after stroke onset. For the segmentation tasks, an attention-gated U-Net was employed. The inputs to the model included DWI, ADC, and thresholded regions with ADC values of less than  $620 \times 10^{-6} \text{ mm}^2/\text{s}$ . The model generated a voxel-by-voxel probability map of tissue infarction as the output. A deep convolutional neural network (CNN) model outperformed the simple ADC thresholding method in predicting the final stroke lesions. It achieved an AUC of 0.91 with a dice similarity coefficient threshold of 0.50, demonstrating its superior performance and accuracy in segmenting the ischemic core.

Moreover, Benzakoun et al<sup>19</sup> conducted a study with the objective of generating synthetic FLAIR images from DWI to assess the DWI-FLAIR mismatch sign as a surrogate for identifying patients who experienced acute ischemic stroke within 4.5 hours of onset. The study included a substantial cohort of 1416 patients. The deep learning model employed in this study was developed based on an edge-aware generative adversarial network (GAN). It was trained on a dataset consisting of DWI, ADC map, and FLAIR images. After completing the training process, synthetic FLAIR images were generated for the test set using the DWI and ADC images. The study's findings demonstrated that by eliminating the need for real FLAIR images in the MRI protocol and instead generating FLAIR images during the acquisition of other sequences, a significant time-saving of approximately 25% can be achieved during scanning. This approach offered a promising strategy for improving efficiency in acute ischemic stroke imaging protocols.

In another work, Verclytte et al<sup>30</sup> conducted a study with the objective of accelerating the acquisition of MRI protocols using deep learning reconstruction techniques. The study involved 173 patients who underwent MRI scans with a 3T scanner in a prospective design. Each patient's MRI protocol consisted of reference acquisitions of T2-FLAIR, DWI, and SWI, which had a total duration of 7 minutes and 54 seconds. Additionally, accelerated multi-shot EPI counterparts for T2-FLAIR and T2\* were obtained, along with a single-shot EPI DWI scan, which had a shorter duration of 1 minute and 54 seconds. To achieve accelerated MRI acquisition, the researchers employed an ultra-fast approach using multiple echo planar imaging (EPI). Furthermore, a new deep learning reconstruction technique was integrated to enhance the signal-to-noise ratio (SNR) of the acquired images. By leveraging this ultra-fast MRI protocol, which included multi-shot EPI counterparts for T2, T2\*, and T2-FLAIR, as well as fast single-shot EPI-based

DWI, the duration of the MRI protocol was reduced by 6 minutes. Importantly, the study found that the differential diagnoses obtained using the accelerated MRI protocol were similar to those obtained with the reference acquisitions.

Besides, Wang et al<sup>39</sup> conducted a study with the objective of delineating the ischemic core and tissue at risk in 3-dimensional (3D) pseudo continuous Arterial Spin Labeling (pCASL) images and DWI, using PWI as the ground truth. The study included a total of 137 patients with acute ischemic stroke, and images were acquired using 1.5 T and 3 T clinical MRI scanners. The hypoperfusion area was identified using  $T_{\text{max}} > 6$  seconds as the ground truth. The researchers employed Highres3DNet,<sup>40</sup> a deep learning algorithm that was trained using CBF and ADC images as well as the label of  $T_{\text{max}}$ . The eligibility for endovascular treatment was retrospectively determined based on the criteria of perfusion/diffusion mismatch in the DEFUSE 3 trial.<sup>9</sup> Subsequently, the trained deep learning algorithm was applied to 12 3D pCASL datasets without fine-tuning of parameters. The algorithm demonstrated the ability to predict the hypoperfusion region defined by dynamic susceptibility contrast in pCASL, achieving a voxel-wise AUC of 0.958.

On top of that, Zhang et al<sup>25</sup> conducted a study with the aim of predicting the onset time of acute ischemic stroke. The study included a total of 422 patients who underwent MRI scans using 1.5 T and 3 T clinical MRI scanners. The inputs for the deep learning architecture consisted of DWI, FLAIR, and T2W MRI. The proposed approach utilized a transfer learning method within the same domain, focusing on adapting the model for an intra-domain task. Initially, the model was trained on a relatively simpler clinical task, specifically stroke detection. This initial training served as a foundation for the subsequent fine-tuning and refinement of the model using various binary thresholds of TSS, aiming to improve its performance and adaptability. The proposed approach was tested using both 2D and 3D deep learning architectures, including an attention-gated pre-trained 2D CNN, 3D U-Net, and 3D CNN trained from scratch. Among these models, the pre-trained 2D CNN achieved the highest performance metrics with a sensitivity of 0.70 and a specificity of 0.81 in classifying TSS of less than 4.5 hours.

Lastly, Qun Zhang et al<sup>23</sup> conducted a study with the objective of predicting the onset time of acute stroke within the intervention window. The study involved 84 patients who underwent MRI scans using a 3 T clinical MRI scanner. Baseline images including ADC, DWI, and T1W MRI were acquired for each patient. To extract relevant information, ROIs were manually segmented on the DWI images. Radiomics features were then extracted from the ADC, DWI, and T1W MRI images based on the segmented ROIs, following image registration. Various preprocessing techniques and feature selection methods were applied to refine the data. Both conventional machine learning algorithms and deep learning algorithms were employed for the classification task. The machine learning algorithms utilized the selected features to predict the onset time of acute stroke, while the deep learning algorithm leveraged the power of neural networks for the same task. Notably, the DL model achieved the highest performance among the different methods tested, achieving an accuracy of 0.72.

## DISCUSSION

The studies included in this review covered different aspects of MR imaging of acute ischemic stroke utilizing machine learning algorithms. The primary objectives of most studies were to predict tissue at risk, identify the ischemic core, and classify patients who experienced



acute ischemic stroke within the treatment window. However, 2 studies had alternative goals, which focused on generating synthetic data<sup>19</sup> and accelerating MR image acquisition.<sup>30</sup>

The extensive utilization of machine learning algorithms in segmentation tasks is of utmost importance in accurately detecting the infarct core from cross-sectional imaging. This is particularly significant as the determination of the infarct core plays a vital role in assessing eligibility for revascularization procedures in treatment.<sup>41</sup> Additionally, given the time-sensitive nature of acute ischemic stroke treatment, it is not surprising that one of the major applications of machine learning has been the identification of patients within the appropriate treatment time window. Various deep learning techniques were employed in these studies, including CNNs, U-Net, autoencoders, and GANs, demonstrating their potentials in segmenting the ischemic core, classifying lesions based on onset time, predicting tissue at risk, and expediting the MRI protocol. The majority of MRI protocols used in these studies primarily included ADC, DWI, FLAIR, and T2W images. The integration of advanced imaging techniques such as PWI and pCASL further improved the accuracy of the deep learning models. However, it is necessary to take into account the increase in total scan time, since a delay of 10 minutes in treatment was reported to cost approximately \$249 million annually in a recent health economics study.<sup>42</sup> Furthermore, the utilization of attention-gated and pretrained networks enhanced the model performances. An attention-gated network selectively focuses on relevant features or regions of an input using an attention mechanism, while a pretrained network refers to a model that has been previously trained on a related task or a large dataset, providing a starting point and improving subsequent model performance. Only 1 study, which was conducted by Zhang et al.,<sup>25</sup> employed intra-domain task adaptive transfer learning to enhance the performance of the model, where the model was initially trained on stroke detection to enhance its performance. The use of machine learning algorithms with deep features has also been reported to enhance accuracy.<sup>34</sup>

## CONCLUSION

The objective of our research is to provide an overview of the latest developments in the utilization of ML algorithms for MRI-based imaging of patients with AIS. The main focus is on how these advancements could potentially be applied in real-world clinical settings. To accomplish this goal, the PRISMA guidelines were followed, and clear inclusion and exclusion criteria were established. A total of 12 relevant papers were identified and included.

To the best of our knowledge, the significance of this study lies in the provision of a novel literature review regarding the utilization of MRI-based machine learning in patients with AIS. Typically, AIS imaging relies on CT scans in the emergency room, with limited use of MRI in this context. Through this review, it is emphasized that MRI, aided by machine learning, may potentially be employed as effectively as CT in the diagnosis and assessment of AIS. The application of AI in MRI of stroke has demonstrated significant progress in tasks such as image segmentation, classification, and prediction. These advancements offer the potential to improve the accuracy and efficiency of stroke diagnosis and treatment planning. However, it is crucial to acknowledge that there is a range of algorithm performances. These variations may be attributed to the use of different accuracy measures, the evaluation of various systems against diverse standards, and the utilization of input data with varying qualities. Such disparities can result in inconsistent and potentially biased differences in study conclusions. To ensure the

robustness of these findings, it is imperative to further validate and generalize the results of AI studies in stroke by including larger and more diverse patient cohorts. In the future, we anticipate witnessing an increased number of ML techniques applied in MRI, particularly with a focus on acute ischemic stroke.

**Peer-review:** Externally peer-reviewed.

**Author Contributions:** Concept – E.O.I.; Design – S.A.; Supervision – E.O.I., E.G.; Resources – E.O.I., S.A.; Materials – S.A.; Data Collection and/or Processing – S.A.; Analysis and/or Interpretation – S.A.; Literature Search – S.A.; Writing Manuscript – S.A.; Critical Review – E.O.I., E.G.

**Declaration of Interests:** Esin Öztürk Işık is an Associate Editor at the Current Research in MRI, however, her involvement in the peer review process was solely as an author. Other authors have no conflicts of interest to declare.

**Funding:** The authors declared that this study has received no financial support.

## REFERENCES

- Ovbiagele B, Nguyen-Huynh MN. Stroke epidemiology: advancing our understanding of disease mechanism and therapy. *Neurotherapeutics*. 2011;8(3):319-329. [\[CrossRef\]](#)
- Soun JE, Chow DS, Nagamine M, et al. Artificial intelligence and acute stroke imaging. *AJNR Am J Neuroradiol*. 2021;42(1):2-11. [\[CrossRef\]](#)
- Boursin P, Paternotte S, Dercy B, Sabben C, Maier B. Semantics, epidemiology and semiology of stroke. *Soins*. 2018;63(828):24-27. [\[CrossRef\]](#)
- Powers WJ, Rabinstein AA, Ackerson T, et al. Guidelines for the early management of patients with acute ischemic stroke: 2019 update to the 2018 guidelines for the early management of acute ischemic stroke: A guideline for healthcare professionals from the American Heart Association/American Stroke Association. *Stroke*. 2019;50(12):e344-e418. [\[CrossRef\]](#)
- Albers GW, Lansberg MG, Kemp S, et al. A multicenter randomized controlled trial of endovascular therapy following imaging evaluation for ischemic stroke (DEFUSE 3). *Int J Stroke*. 2017;12(8):896-905. [\[CrossRef\]](#)
- Tsivgoulis G, Katsanos AH, Sandset EC, et al. Thrombolysis for acute ischaemic stroke: current status and future perspectives. *Lancet Neurol*. 2023;22(5):418-429. [\[CrossRef\]](#)
- Saver JL. Time is brain—quantified. *Stroke*. 2006;37(1):263-266. [\[CrossRef\]](#)
- Liebeskind DS, Saber H, Xiang B, et al. Collateral circulation in thrombectomy for stroke after 6 to 24 hours in the DAWN trial. *Stroke*. 2022;53(3):742-748. [\[CrossRef\]](#)
- Albers GW, Marks MP, Kemp S, et al. Thrombectomy for stroke at 6 to 16 hours with selection by perfusion imaging. *N Engl J Med*. 2018;378(8):708-718. [\[CrossRef\]](#)
- Nogueira RG, Jadhav AP, Haussen DC, et al. Thrombectomy 6 to 24 hours after stroke with a mismatch between deficit and infarct. *N Engl J Med*. 2018;378(1):11-21. [\[CrossRef\]](#)
- Elfil M, Eldokmak M, Baratloo A, Ahmed N, Amin HP, Koo BB. Pathophysiological mechanisms, neuroimaging and treatment in wake-up stroke. *CNS Spectr*. 2020;25(4):460-467. [\[CrossRef\]](#)
- Srinivasan A, Goyal M, Al Azri F, Lum C. State-of-the-art imaging of acute stroke. *RadioGraphics*. 2006;26(suppl 1):S75-S95. [\[CrossRef\]](#)
- Rimmele DL, Thomalla G. Wake-up stroke: clinical characteristics, imaging findings, and treatment option - an update. *Front Neurol*. 2014;5:35. [\[CrossRef\]](#)
- Thomalla G, Simonsen CZ, Boutitie F, et al. MRI-guided thrombolysis for stroke with unknown time of onset. *N Engl J Med*. 2018;379(7):611-622. [\[CrossRef\]](#)
- Thomalla G, Cheng B, Ebinger M, et al. DWI-FLAIR mismatch for the identification of patients with acute ischaemic stroke within 4.5 h of symptom onset (PRE-FLAIR): a multicentre observational study. *Lancet Neurol*. 2011;10(11):978-986. [\[CrossRef\]](#)
- Menon BK, Almekhlafi MA, Pereira VM, et al. Optimal workflow and process-based performance measures for endovascular therapy in acute ischemic stroke: analysis of the solitaire FR thrombectomy for acute revascularization study. *Stroke*. 2014;45(7):2024-2029. [\[CrossRef\]](#)
- Nael K, Khan R, Choudhary G, et al. Six-minute magnetic resonance imaging protocol for evaluation of acute ischemic stroke: pushing the boundaries. *Stroke*. 2014;45(7):1985-1991. [\[CrossRef\]](#)

18. Sheth SA, Jahan R, Gralla J, et al. Time to endovascular reperfusion and degree of disability in acute stroke. *Ann Neurol*. 2015;78(4):584-593. [\[CrossRef\]](#)
19. Benzakoun J, Deslys MA, Legrand L, et al. Synthetic FLAIR as a substitute for FLAIR sequence in acute ischemic stroke. *Radiology*. 2022;303(1):153-159. [\[CrossRef\]](#)
20. Liu CF, Hsu J, Xu X, et al. Deep learning-based detection and segmentation of diffusion abnormalities in acute ischemic stroke. *Commun Med (Lond)*. 2021;1:61. [\[CrossRef\]](#)
21. Jiang L, Zhang C, Wang S, et al. MRI Radiomics features from infarction and cerebrospinal fluid for prediction of cerebral edema after acute ischemic stroke. *Front Aging Neurosci*. 2022;14:782036. [\[CrossRef\]](#)
22. Li BM, Castorina LV, Valdés Hernández MDC, et al. Deep attention super-resolution of brain magnetic resonance images acquired under clinical protocols. *Front Comput Neurosci*. 2022;16:887633. [\[CrossRef\]](#)
23. Zhang YQ, Liu AF, Man FY, et al. MRI radiomic features-based machine learning approach to classify ischemic stroke onset time. *J Neurol*. 2022;269(1):350-360. [\[CrossRef\]](#)
24. Ho KC, Speier W, Zhang H, Scalzo F, El-Saden S, Arnold CW. A machine learning approach for classifying ischemic stroke onset time from imaging. *IEEE Trans Med Imaging*. 2019;38(7):1666-1676. [\[CrossRef\]](#)
25. Zhang H, Polson JS, Nael K, et al. Intra-domain task-adaptive transfer learning to determine acute ischemic stroke onset time. *Comput Med Imaging Graph*. 2021;90:101926. [\[CrossRef\]](#)
26. Jiang F, Jiang Y, Zhi H, et al. Artificial intelligence in healthcare: past, present and future. *Stroke Vasc Neurol*. 2017;2(4):230-243. [\[CrossRef\]](#)
27. Nagel S, Sinha D, Day D, et al. e-ASPECTS software is non-inferior to neuroradiologists in applying the ASPECT score to computed tomography scans of acute ischemic stroke patients. *Int J Stroke*. 2017;12(6):615-622. [\[CrossRef\]](#)
28. Herweh C, Ringleb PA, Rauch G, et al. Performance of e-ASPECTS software in comparison to that of stroke physicians on assessing CT scans of acute ischemic stroke patients. *Int J Stroke*. 2016;11(4):438-445. [\[CrossRef\]](#)
29. Guberina N, Dietrich U, Radbruch A, et al. Detection of early infarction signs with machine learning-based diagnosis by means of the Alberta Stroke Program Early CT score (ASPECTS) in the clinical routine. *Neuroradiology*. 2018;60(9):889-901. [\[CrossRef\]](#)
30. Vercllytte S, Gnanih R, Verdun S, et al. Ultrafast MRI using deep learning echo planar imaging for a comprehensive assessment of acute ischemic stroke. *Eur Radiol*. 2023;33(5):3715-3725. [\[CrossRef\]](#)
31. Zhu H, Jiang L, Zhang H, Luo L, Chen Y, Chen Y. An automatic machine learning approach for ischemic stroke onset time identification based on DWI and FLAIR imaging. *NeuroImage Clin*. 2021;31:102744. [\[CrossRef\]](#)
32. Tan M, Le Q. *Efficient Net: rethinking model scaling for convolutional neural networks*. International conference on machine learning [\[CrossRef\]](#) 2019. <http://proceedings.mlr.press/v97/tan19a.html?ref=jina-ai-gmbh.ghost.io>
33. van Griethuysen JJM, Fedorov A, Parmar C, et al. Computational Radiomics system to decode the radiographic phenotype. *Cancer Res*. 2017;77(21):e104-e107. [\[CrossRef\]](#)
34. Ho KC, Speier W, El-Saden S, Arnold CW. Classifying acute ischemic stroke onset time using deep imaging features. *AMIA Annu Symp Proc*. 2017;2017:892-901. <https://www.ncbi.nlm.nih.gov/pmc/articles/PMC5977679>
35. Yu Y, Xie Y, Thamm T, et al. Use of deep learning to predict final ischemic stroke lesions from initial magnetic resonance imaging. *JAMA Netw Open*. 2020;3(3):e200772. [\[CrossRef\]](#)
36. Yu Y, Xie Y, Thamm T, et al. Tissue at risk and ischemic core estimation using deep learning in acute stroke. *AJNR Am J Neuroradiol*. 2021;42(6):1030-1037. [\[CrossRef\]](#)
37. Do LN, Baek BH, Kim SK, Yang HJ, Park I, Yoon W. Automatic assessment of ASPECTS using diffusion-weighted imaging in acute ischemic stroke using recurrent residual convolutional neural network. *Diagnostics (Basel)*. 2020;10(10). [\[CrossRef\]](#)
38. Nazari-Farsani S, Yu Y, Duarte Armindo R, et al. Predicting final ischemic stroke lesions from initial diffusion-weighted images using a deep neural network. *NeuroImage Clin*. 2023;37:103278. [\[CrossRef\]](#)
39. Wang K, Shou Q, Ma SJ, et al. Deep learning detection of penumbral tissue on arterial spin labeling in stroke. *Stroke*. 2020;51(2):489-497. [\[CrossRef\]](#)
40. Niethammer M, Styner M, Aylward S, et al. Information Processing in Medical Imaging: 25th International Conference, IPMI 2017, Boone, NC, USA, June 25-30, 2017, Proceedings [\[CrossRef\]](#) Springer; 2017. <https://play.google.com/store/books/details?id=r8gmDwAAQBAJ>
41. Catanese L, Tarsia J, Fisher M. Acute ischemic stroke therapy overview. *Circ Res*. 2017;120(3):541-558. [\[CrossRef\]](#)
42. Kunz WG, Hunink MG, Almekhlafi MA, et al. Public health and cost consequences of time delays to thrombectomy for acute ischemic stroke. *Neurology*. 2020;95(18):e2465-e2475. [\[CrossRef\]](#)

# Diagnosis of Caroli Disease with Gadoxetic Acid-Enhanced Magnetic Resonance Imaging

Ramazan Orkun Önder<sup>ID</sup>, Serdar Aslan<sup>ID</sup>, Tumay Bekci<sup>ID</sup>

Department of Radiology, Giresun University Faculty of Medicine, Giresun, Turkey

**Cite this article as:** Önder RO, Aslan S, Bekci T. Diagnosis of caroli disease with gadoxetic acid-enhanced magnetic resonance imaging. *Current Research in MRI*, 2024;3(1):27-29.

**Corresponding author:** Ramazan Orkun Önder, e-mail: orkunonder535@gmail.com

**Received:** July 25, 2023 **Revision Requested:** August 14, 2023 **Last Revision Received:** August 16, 2023 **Accepted:** August 16, 2023

**Publication Date:** September 4, 2023

DOI:10.5152/CurrResMRI.2023.23067



Content of this journal is licensed under a Creative Commons Attribution-NonCommercial 4.0 International License.

## Abstract

Caroli disease (CD) is a condition in which there are multiple cystic dilations of the bile ducts within the liver that are present from birth. In this case report, we present the imaging findings of a 33-year-old woman who was diagnosed noninvasively after gadoxetic acid (GA)-enhanced magnetic resonance imaging, which has been used in recent years, which is very rare in the literature. A woman, aged 33, was admitted to the hospital after experiencing recurring episodes of pain in the upper right area of her abdomen for a long period of time. Laboratory tests showed elevated liver enzyme levels and hyperbilirubinemia. Abdominal ultrasonography revealed cystic lesions in the liver and mild enlargement of the common bile duct. It was observed that cystic lesions in the liver filled with GA in the hepatobiliary phase and were associated with the intrahepatic bile ducts. Thus, the patient was diagnosed with CD. In the hepatobiliary phase, GA-enhanced magnetic resonance imaging allows the detection of other conditions in which a central dot sign (CDS) occurs (e.g., peribiliary cysts, periportal lymphedema, and jaundice due to biliary obstruction) and noninvasive diagnosis of CD in the absence of a CDS.

**Keywords:** Caroli disease, central dot sign, gadoxetic acid, hepatobiliary phase, MRI

## INTRODUCTION

Caroli disease (CD) is a condition in which there are multiple cystic dilations of the bile ducts within the liver that are present from birth. Caroli disease can manifest as either diffuse or limited, and it can involve the formation of sac-like structures that connect with the biliary tree and form cystic formations. They are also classified as a type V choledochal cyst, according to the Todani classification.<sup>1</sup> Two categories of magnetic resonance imaging (MRI) contrast agents possess hepatocyte-selective characteristics: gadolinium-based and manganese-based agents. While gadolinium-based agents exhibit both hepatocyte and perfusion imaging properties, making them bimodal contrast agents, gadoxetic acid (GA) is a gadolinium-based hepatocyte-specific contrast agent.<sup>2</sup> In this case report, we present the imaging findings of a 33-year-old woman who was diagnosed with CD noninvasively after GA-enhanced MRI, which has been used in recent years, which is very rare in the literature.

## CASE PRESENTATION

A woman, aged 33, was admitted to the hospital due to experiencing recurring episodes of pain in the upper right area of her abdomen for a long period of time. Her medical history was unremarkable. Upon physical examination, mild tenderness in the right upper quadrant was revealed. Laboratory results demonstrated elevated aspartate aminotransferase of 310 U/L (normal < 40 U/L), alanine aminotransferase of 207 units/L (normal < 41 U/L), direct bilirubin of 3.11 mg/dL (normal < 0.2 mg/dL), and total bilirubin of 4.67 mg/dL (normal < 1.25 mg/dL). Abdominal ultrasonography (US) revealed cystic lesions in the liver and mild enlargement of the common bile duct. The patient then underwent GA-enhanced MRI. Cystic lesions with high signal on T2-weighted MRI and low signal on T1-weighted MRI were observed in liver segments 4, 7, and 8 (the largest was 3 × 2 cm in segment 7) (Figure 1). Contrast enhancement was not observed in cystic lesions in venous-phase contrast MRI (Figure 2). Magnetic resonance imaging in the hepatobiliary phase of the liver 20 minutes after GA injection showed cystic lesions filled with GA (Figure 3). Thus, the patient was noninvasively diagnosed with CD and found to have an episode of cholangitis. The patient had no findings of hepatomegaly, splenomegaly, or portal hypertension. The patient was started on ursodeoxycholic acid 250 mg daily as supportive therapy, and conservative treatment for cholangitis and follow-up was recommended. Written informed consent was obtained from the patient who participated in this study.

## DISCUSSION

Caroli disease may be focal or diffuse and it is important to distinguish diffuse CD from autosomal dominant polycystic liver disease or peribiliary cysts in a cirrhotic liver. In terms of MR imaging findings, CD is characterized by multiple cysts within the liver, closely associated with the biliary system, often with a central dot sign (CDS).<sup>3</sup> While MRI may not show the communication between cystic lesions and draining bile ducts, this challenge can be overcome by utilizing GA-enhanced MRI. This advanced technique allows for the visualization of communications between cystic lesions and draining bile ducts, enabling the differentiation of CD from other conditions such as autosomal

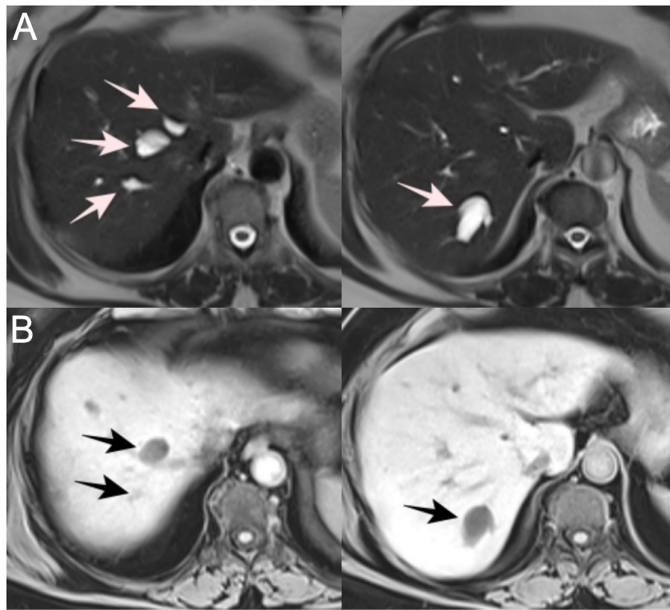


**Figure 1.** (A) High-signal cystic lesions (open arrows) in the liver observed on T2-weighted MRI. (B) Low-signal cystic lesions (filled arrows) in the liver observed on T1-weighted MRI. MRI, magnetic resonance imaging.

dominant polycystic liver disease or peribiliary cysts in a cirrhotic liver.<sup>4,5</sup> Various imaging techniques consistently reveal similar findings, with ultrasound being the initial test of choice, showing the presence of saccular dilatations in the intrahepatic ducts.<sup>6,7</sup> The CDS, which was not detected in our case, is a clue for the diagnosis of CD. The CDS represents the telltale appearance of intrahepatic portal vein branches surrounded by severely dilated bile ducts, which can be visualized by either computed tomography, MRI, or US. However, it may not be seen in every patient, and while initially considered specific for this disease, later results have shown that the CDS sporadically also occurs in other conditions (e.g., peribiliary cysts, periportal lymphedema, and jaundice due to biliary obstruction).<sup>8-10</sup> Cholangiography by endoscopic retrograde cholangiopancreatography (ERCP) shows nonocclusive cystic dilatations communicating with the biliary tree. However, invasive methods (e.g., ERCP and percutaneous transhepatic cholangiography) can have complications such as bleeding, infection, and pancreatitis. After venous injection of GA, up to 50% is taken up exclusively by

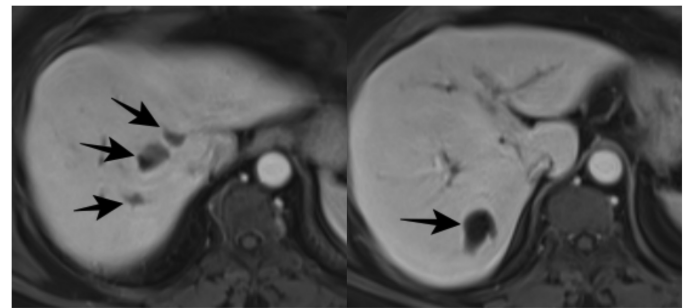


**Figure 2.** Nonenhancing cystic lesions (filled arrows) observed on venous-phase contrast-enhanced MRI. MRI, magnetic resonance imaging.

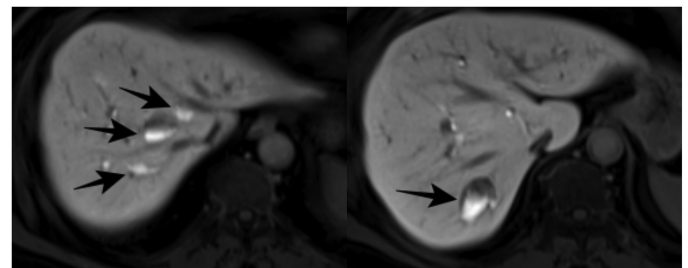


**Figure 3.** In the hepatobiliary phase, cystic lesions filled with GA (filled arrows) and associated with intrahepatic bile ducts. GA, gadoxetic acid.

organic anion transporter polypeptides in the sinusoidal membrane of normal hepatocytes and then excreted into the biliary ducts.<sup>11</sup> The increase in liver parenchyma is determined by the balance of this transport mechanism and an optimal enhancement effect is observed for a period of 10-40 minutes after administration.<sup>12</sup> In recent years, it has been suggested that the use of contrast-enhanced MRI with GA allows a safe, noninvasive diagnosis of CD.<sup>10,13-14</sup> In our case, we diagnosed CD after GA-enhanced MRI without the use of invasive methods. In conclusion, in the hepatobiliary phase, GA-enhanced MRI allows the detection of other conditions in which CDS occurs (e.g., peribiliary cysts, periportal lymphedema, and jaundice due to biliary obstruction) and enables the noninvasive diagnosis of CD even in the absence of a CDS. This approach also protects patients from the complications of invasive procedures (e.g., ERCP and percutaneous transhepatic cholangiography) such as bleeding, infection, and pancreatitis.

**Informed Consent:** Written informed consent was obtained from patient who participated in this study.

**Peer-review:** Externally peer-reviewed.

**Author Contributions:** Concept – R.O.Ö.; Design – R.O.Ö., S.A.; Supervision – R.O.Ö., T.B.; Resources – R.O.Ö.; Materials – S.A., T.B.; Data Collection and/or Processing – R.O.Ö., T.B.; Analysis and/or Interpretation – R.O.Ö., S.A.; Literature Search – S.A., T.B.; Writing Manuscript – R.O.Ö.; Critical Review – R.O.Ö., T.B.; Other – S.A., T.B.

**Declaration of Interests:** The authors have no conflict of interest to declare.

**Funding:** The authors declared that this study has received no financial support.

## REFERENCES

1. Singham J, Yoshida EM, Scudamore CH. Choledochal cysts: part 2 of 3: Diagnosis. *Can J Surg.* 2009;52(6):506-511.

## MAIN POINTS

- Central dot sign may be a clue for Caroli disease (CD). However, it is not specific for this disease. Because it may also occur sporadically in conditions such as peribiliary cysts, periportal lymphedema, and jaundice due to biliary obstruction.
- Ultrasonography and computed tomography may not clearly distinguish dilatation of intrahepatic bile ducts from cystic lesions. However, on magnetic resonance imaging (MRI) with gadoxetic acid (GA) in the hepatobiliary phase, dilatation of the intrahepatic bile ducts can be easily detected as cystic lesions filled with the contrast medium.
- Gadaxetic acid-enhanced MRI in the hepatobiliary phase enables non-invasive diagnosis of CD, protecting patients from the complications of invasive procedures.



2. Ba-Ssalamah A, Uffmann M, Saini S, Bastati N, Herold C, Schima W. Clinical value of MRI liver-specific contrast agents: a tailored examination for a confident non-invasive diagnosis of focal liver lesions. *Eur Radiol.* 2009;19(2):342-357. [\[CrossRef\]](#)
3. Levy AD, Rohrmann CA Jr, Murakata LA, Loneragan GJ. Caroli's disease: radiologic spectrum with pathologic correlation. *AJR Am J Roentgenol.* 2002;179(4):1053-1057. [\[CrossRef\]](#)
4. Park MS, Kim BC, Kim T, Kim MJ, Kim KW. Double common bile duct: curved-planar reformatted computed tomography (CT) and gadobenate dimeglumine-enhanced MR cholangiography. *J Magn Reson Imaging.* 2008;27(1):209-211. [\[CrossRef\]](#)
5. Park MS, Yu JS, Lee JH, Kim KW. Value of manganese-enhanced T1- and T2-weighted MR cholangiography for differentiating cystic parenchymal lesions from cystic abnormalities which communicate with bile ducts. *Yonsei Med J.* 2007;48(6):1072-1074. [\[CrossRef\]](#)
6. Yamaguchi T, Cristaudi A, Kokudo T, Uldry E, Demartines N, Halkic N. Surgical treatment for monolobular Caroli's disease – report of a 30-year single center case series. *BioSci Trends.* 2018;12(4):426-431. [\[CrossRef\]](#)
7. Soares KC, Goldstein SD, Ghaseb MA, Kamel I, Hackam DJ, Pawlik TM. Pediatric choledochal cysts: diagnosis and current management. *Pediatr Surg Int.* 2017;33(6):637-650. [\[CrossRef\]](#)
8. Khalefa AA, Alrasheed M, Saeedan MB. Central dot sign. *Abdom Radiol.* 2016;41(11):2289-2290. [\[CrossRef\]](#)
9. Santiago I, Loureiro R, Curvo-Semedo L, et al. Congenital cystic lesions of the biliary tree. *AJR Am J Roentgenol.* 2012;198(4):825-835. [\[CrossRef\]](#)
10. Salvadori PS, Torres US, D'Ippolito G. Contrast-enhanced magnetic resonance cholangiography with gadoteric-acid-disodium for the detection of biliary-cyst communication in Caroli disease. *Gastroenterol Hepatol.* 2016;39(10):669-670. [\[CrossRef\]](#)
11. Van Beers BE, Pastor CM, Hussain HK. Primovist, Eovist: what to expect? *J Hepatol.* 2012;57(2):421-429. [\[CrossRef\]](#)
12. Brismar TB, Dahlstrom N, Edsberg N, Persson A, Smedby O, Albiin N. Liver vessel enhancement by Gd-BOPTA and Gd-EOB-DTPA: a comparison in healthy volunteers. *Acta Radiol.* 2009;50(7):709-715. [\[CrossRef\]](#)
13. Choi BI, Yeon KM, Kim SH, Han MC. Caroli disease: central dot sign in CT. *Radiology.* 1990;174(1):161-163. [\[CrossRef\]](#)
14. Ahmadi T, Itai Y, Minami M. Central dot sign in entities other than Caroli disease. *Radiat Med.* 1997;15(6):381-384.

# A Rare Coupling: Central Tuberculous and Brucella Co-infection

Önder Durmaz<sup>1</sup>, Gönül Seven Yalçın<sup>2</sup>, Umut Devrim Binay<sup>3</sup>, Mecdi Gürhan Balcı<sup>4</sup>, Türkhun Çetin<sup>4</sup>, Edhem Ünver<sup>5</sup>

<sup>1</sup>Department of Radiology, Erzincan Binali Yıldırım University Faculty of Medicine, Erzincan, Turkey

<sup>2</sup>Department of Chest Disease, Süleyman Demirel University Faculty of Medicine, Erzincan, Turkey

<sup>3</sup>Department of Infectious Diseases, Erzincan Binali Yıldırım University Faculty of Medicine, Erzincan, Turkey

<sup>4</sup>Erzincan Binali Yıldırım University Faculty of Medicine, Erzincan, Turkey

<sup>5</sup>Department of Chest Disease, Erzincan Binali Yıldırım University Faculty of Medicine, Erzincan, Turkey

**Cite this article as:** Durmaz Ö, Seven Yalçın G, Devrim Binay U, Gürhan Balcı M, Çetin T, Ünver E. A rare coupling: Central tuberculous and brucella co-infection. *Current Research in MRI*, 2024;3(1):30-32.

**Corresponding author:** Önder Durmaz, e-mail: dronzonder2577@gmail.com

**Received:** August 10, 2023 **Revision Requested:** August 29, 2023 **Last Revision Received:** August 29, 2023 **Accepted:** September 1, 2023

**Publication Date:** September 29, 2023

DOI:10.5152/CurrResMRI.2023.23070



Content of this journal is licensed under a Creative Commons Attribution-NonCommercial 4.0 International License.

## Abstract

Tuberculosis and brucellosis can imitate each other in terms of clinical and laboratory findings, but their co-infection is rarely reported. The current case report will present such an uncommon co-infection. A 56-year-old farmer was admitted with complaints of disorientation and weight loss. He was infected with both tuberculosis and brucellosis. Cervical lymph node biopsy confirmed the diagnosis of tuberculosis, and hemagglutination test verified the diagnosis of brucellosis. Although tuberculous meningitis clinic is known to have a severe course, its coexistence with brucella infection should be investigated in instances that do not respond to therapy.

**Keywords:** Brucellosis, infection, meningitis, tuberculosis

## INTRODUCTION

Tuberculosis (TB) is one of the most prevalent and older causes of infection. It is also endemic in Turkey. Tuberculosis most commonly affects the lungs, followed by lymph nodes and pleura. Although central nervous system (CNS) involvement is uncommon (about 1%), it has a significant mortality (particularly in TB meningitis). Brucella infection (brucellosis) is a zoonotic disease prevalent in developing countries, particularly rural regions. Brucellosis and TB can imitate each other in terms of clinical and laboratory findings, but their co-infection is rarely

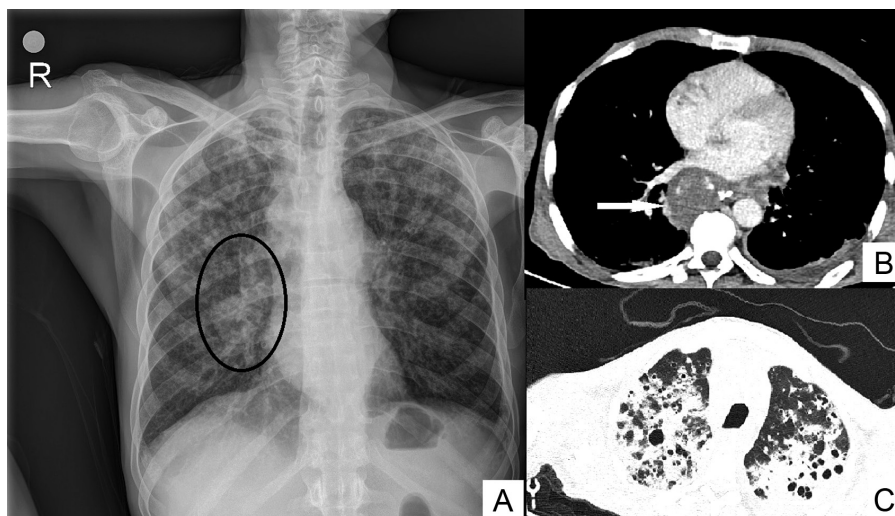


**Figure 1.** Reticulonodular densities at the upper and mid zones and right hilar prominence (A, circle) can be seen on chest X-ray (A). Right hilar fullness corresponds to a calcified lymph node on computerized tomography image (B, arrow). Consolidations, ground glass opacities, bronchiectasis, and cystic changes can be seen at bilateral upper lobes on computerized tomography image (C).

reported.<sup>1,2</sup> In the current case report, such an uncommon co-infection will be discussed.

### CASE PRESENTATION

A 56-year-old farmer was admitted to our outpatient clinic after complaints of weight loss and confusion over the previous 2 weeks. In the patient's history, he had no chronic disease and had lost 15 kilograms in the previous. On physical examination, he was disoriented; body temperature was 38.6 degrees; arterial blood pressure was 120/80 mmHg; cardiac rate was 90/min; respiratory sounds were weak on auscultation; and minimal rales were present in the bilateral lung bases. Laboratory findings were: leukocytes, 17800  $\mu$ L; lymphocytes, 70  $\mu$ L (0.40%); neutrophils, 15530  $\mu$ L (87.20%); C reactive protein (CRP), 152 mg/L; sedimentation, 92; sodium (Na), 126 mmol/L; potassium (K), 3.2 mmol/L; lactate dehydrogenase, 327 u/L. Cultures (blood, urine, and sputum) were obtained, but they came out negative, and broad-spectrum antibiotic therapy was then started. Posteroanterior chest X-ray showed reticulonodular densities in the upper and middle zones and right hilar prominence (Figure 1). Due to patient's recent cognitive impairment, a cranial magnetic resonance imaging (MRI) was performed; findings consistent with meningoencephalitis was seen in the temporoparietal region (Figure 2). Sonographically, widespread lymphadenopathy (LAP) was seen in the neck and abdomen (Figure 3). An excisional biopsy was taken from one of the posterior cervical LAPs; the histopathological diagnosis was compatible with TB (caseified granulomatous inflammation, Figure 4), and the patient was then started on antituberculosis treatment. Lumbar puncture was performed on the patient in the second week of treatment due to droopy left eyelid. The cerebrospinal fluid (CSF) analysis indicated negative acid-resistant bacilli (ARB) and culture was also negative, but 200/mm<sup>3</sup> leukocytes were found. Some suspicious bacillus was observed by using the Ehrlich-Ziehl-Neelsen staining method. With these findings, the patient's diagnosis of tuberculous meningitis was confirmed, and dexamethasone was added to his treatment. In the follow-up MRI, regression was identified in his previous lesions. Despite the fact that the lesions had decreased, the brucellosis test was requested because the patient's state of consciousness remained impaired. The test result was positive. Brucellosis treatment was initiated for the patient (doxycycline 100 mg 2  $\times$  1). Following the treatment, a clinical improvement was obtained. Radiological improvement was accelerated. Improvements in the patient's laboratory results were also seen (leukocyte: 9500  $\mu$ L, lymphocyte: 570 (6%)  $\mu$ L, neutrophil: 7530 (79.40%)  $\mu$ L CRP: 10 mg/L). It was decided to continue the co-infection treatment and to monitor the patient

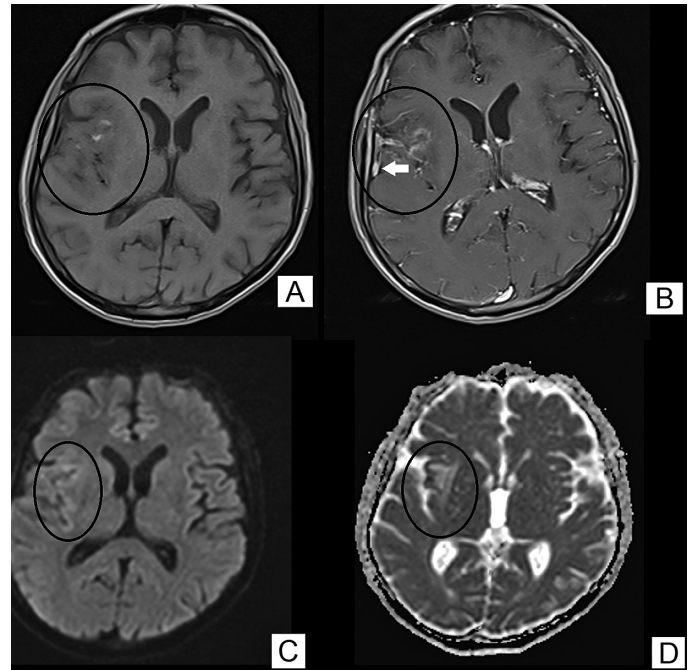


**Figure 2.** Gyral enhancement (A, B, circles), meningeal thickening, and enhancement (B, arrow) is present at right temporoparietal region on pre- (A) and post contrast (B) T1 weighted images. On diffusion-weighted image (C) and Apparent Diffusion Coefficient (ADC) map (D), mild gyral diffusion restriction is also present at the same level (C, D, circles).

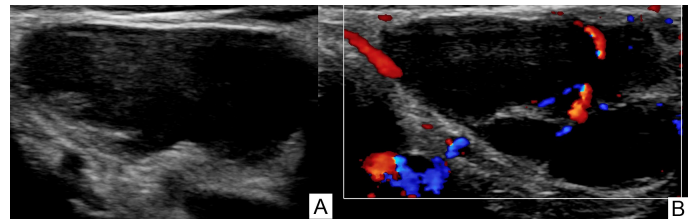


**Figure 3.** Cervical lymphadenopathies.(A) Both hilar and peripheral vascularization are present in the color Doppler ultrasonographic image (B).

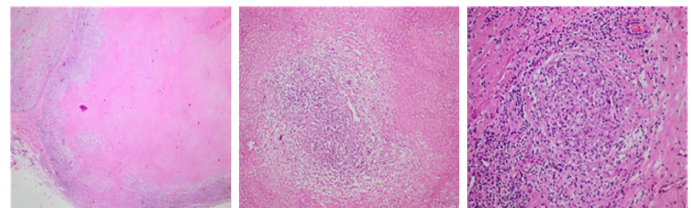


**Figure 4.** Specimens of pathological lymph node stained with hematoxylin-eosin and magnified calcified granulomas on thin paraffin sections at 40 $\times$  magnification.

at regular intervals as an outpatient. After the patient's personal data were anonymized, he approved the sharing of his data on the related disease. Written informed consent was obtained from the patient who agreed to take part in the study.

### DISCUSSION

Tuberculous meningitis is the most prevalent type of TB of the CNS. The leptomeninges are infected when a person has tuberculous

### MAIN POINTS

- Tuberculosis (TB) is still the most important public health problem in developing countries.
- In order to diagnose tuberculosis, it should be kept in mind in the differential diagnosis, and clinical and laboratory findings supporting TB should be known.
- In cases that are resistant to treatment, co-infections should definitely be investigated.
- Multisystemic complications, which cause serious morbidity and mortality, develop in untreated brucella cases. This leads to worse treatment results if co-infection with TB exists.

meningitis, which is the most prevalent symptom of intracranial TB. Tuberculous pachymeningitis is the name for this condition, which is less likely to affect only the dura mater. Difficulties with diagnosis and treatment lead to an increased mortality and morbidity.<sup>3,4</sup> The rates of ARB positivity in CSF in tuberculous meningitis ranges between 10% and 40%.<sup>5</sup> Similarly, ARB was negative in our case, and no growth was detected in the cultures. The diagnosis of the patient was made by clinical, laboratory, radiological, and histopathological findings. Prompt treatment for tuberculous meningitis is critical. The delay in hospitalization caused difficulties in the clinical response. Brucella is a multisystem disease like TB that can camouflage itself very well with some of its findings and can be transmitted by animal products. Sometimes even suspicion is enough to make its diagnosis. Our patient was a farmer. Once again, we understand the importance of a detailed anamnesis in diagnosing an occupational disease. The absence of clinical response despite treatment suggested the presence of co-infection. The clinical response was obtained after positive Brucella test and subsequently revised treatment.

Although TB and brucellosis are both frequent diseases in developing countries, their coexistence is uncommon. Even though it is well known that tuberculous meningitis has a severe course, the existence of co-infection should definitely be explored in cases when treatment is not effective. The benefit of early diagnosis and treatment can be seen with reduced mortality/morbidity.

**Informed Consent:** Written informed consent was obtained from the patient who agreed to take part in the study.

**Peer-review:** Externally peer-reviewed.

**Author Contributions:** Conception – Ö.D., G.S.Y.; Design – Ö.D., T.Ç.; Supervision – Ö.D., E.Ü.; Materials – Ö.D., T.Ç., M.G.B.; Data Collection and/or Processing – Ö.D., M.G.B., T.Ç.; Analysis and/or Interpretation – Ö.D., M.G.B., E.Ü.; Literature Review – Ö.D., G.S.Y.; Writing Manuscript – Ö.D., G.S.Y., U.D.B.; Critical Review – Ö.D., U.D.B.

**Declaration of Interests:** The authors have no conflicts of interest to declare.

**Funding:** The authors declared that this study has received no financial support.

## REFERENCES

1. Thwaites GE, Schoeman JF. Update on tuberculosis of the central nervous system: pathogenesis, diagnosis, and treatment. *Clin Chest Med.* 2009;30(4):745-754. [\[CrossRef\]](#)
2. Akdeniz H, Irmak H, Anlar O, Demiröz AP. Central nervous system brucellosis: presentation, diagnosis and treatment. *J Infect.* 1998;36(3):297-301. [\[CrossRef\]](#)
3. Karsen H, Karahocagil MK, Irmak H, Demiröz AP. A meningitis case of Brucella and tuberculosis co-infection. *Mikrobiyol Bul.* 2008;42(4): 689-694.
4. Hosoglu S, Geyik MF, Balık I, et al. Predictors of outcome in patients with tuberculous meningitis. *Int J Tuberc Lung Dis.* 2002;6(1):64-70.
5. Avcı M, Özgenç O, Arı A, Mermut G. Tüberküloz menenjit olgularının değerlendirilmesi. *İnfeksiyon Derg.* 2007;21:117-122.



# Challenges in Magnetic Resonance Imaging Anesthesia Findings and Recommendations

Hakan Gökalp Taş 

Department of Anesthesiology and Reanimation, Erzincan Binali Yıldırım University Faculty of Medicine, Erzincan, Turkey

**Cite this article as:** Taş HG. Challenges in magnetic resonance imaging anesthesia findings and recommendations. *Current Research in MRI*, 2024;3(1):33-34.

**Corresponding author:** Hakan Gökalp Taş, e-mail: hakangokalptas@hotmail.com

**Received:** January 30, 2024 **Revision Requested:** February 7, 2024 **Last Revision Received:** February 7, 2024 **Accepted:** February 17, 2024

**Publication Date:** March 21, 2024

DOI:10.5152/CurrResMRI.2024.24093



Content of this journal is licensed under a Creative Commons Attribution-NonCommercial 4.0 International License.

To the Editor,

Nowadays, the number of magnetic resonance imaging (MRI) centers is growing daily as a result of technological advancements, the growing number of MRI centers, and the growing importance of MRI in diagnosis and treatment due to its improved quality and accessibility. The number of patients requiring anesthesia rises along with the demand for MR imaging. This letter aims to highlight the difficulties associated with anesthesia during magnetic resonance imaging.

Challenges regarding the physical location of the MRI device:

The MRI unit provides particular challenges because it is usually located outside of the operating room, requires specialist equipment of its own, and takes longer to prepare than a standard surgery.<sup>1,2</sup>

Communication challenges:

The existence of teams that do not collaborate frequently, the darkness of the room, the distance between the patient and the doctor, the loud noise level drowning out other devices' sounds and making them difficult to hear, and other factors are the causes of communication issues.<sup>3,4</sup>

Environmental risks and challenges:

Even heavy items, such as oxygen or nitrous oxide tanks, could unintentionally shoot projectiles into the scanner's bore due to the powerful static magnetic field.<sup>4,5</sup> In addition to heating tissue or devices, radiofrequency energy can create current in conductors including fluid-filled tubing, equipment cables, and electrocardiogram (ECG) leads.<sup>4</sup> Strong magnetic fields and radiofrequency radiation can produce artifacts that make it more difficult to interpret pressure waveforms or ECGs clinically.<sup>6</sup>

An evaluation of all of them reveals that anesthesia during MRI is now a method with its own inherent dynamics, requiring skill and cautious execution.

**Peer-review:** Externally peer-reviewed.

**Declaration of Interests:** The author has no conflict of interest to declare.

**Funding:** The author declared that this study has received no financial support.

## REFERENCES

1. Deen J, Vandevivere Y, Van de Putte P. Challenges in the anesthetic management of ambulatory patients in the MRI suites. *Curr Opin Anaesthesiol*. 2017;30(6):670-675. [\[CrossRef\]](#)
2. Boggs SD, Barnett SR, Urman RD. The future of nonoperating room anesthesia in the 21st century: emphasis on quality and safety. *Curr Opin Anaesthesiol*. 2017;30(6):644-651. [\[CrossRef\]](#)
3. Berkow LC. Anesthetic management and human factors in the intraoperative MRI environment. *Curr Opin Anaesthesiol*. 2016;29(5):563-567. [\[CrossRef\]](#)
4. Wilson SR, Shinde S, Appleby I, et al. Guidelines for the safe provision of anaesthesia in magnetic resonance units 2019: guidelines from the Association of Anaesthetists and the Neuro Anaesthesia and Critical Care Society of Great Britain and Ireland. *Anaesthesia*. 2019;74(5):638-650. [\[CrossRef\]](#)

5. American Society of Anesthesiologists Task Force on Intraoperative Awareness. Practice advisory for intraoperative awareness and brain function monitoring: a report by the American society of anesthesiologists task force on intraoperative awareness. *Anesthesiology*. 2006;104(4):847-864. [\[CrossRef\]](#)
6. Schroeck H, Welch TL, Rovner MS, Johnson HA, Schroeck FR. Anesthetic challenges and outcomes for procedures in the intraoperative magnetic resonance imaging suite: a systematic review. *J Clin Anesth*. 2019;54:89-101. [\[CrossRef\]](#)